Qubit chains' emergent behaviour from biologically-inspired dynamics

Xavier Laurent

A thesis presented for the degree of
MSc Physics (by research)

UNIVERSITY
of York

Department of Physics
York University UK
2025

Contents

Abstract

Building upon the investigation "A model of interacting quantum neurons with a dynamic synapse" by Torres and Manzano (2022) that explored the emergent behaviour of a two-qubit quantum systems through biologically inspired qubit interaction, our research introduces a significant extension.

We expand the original model to explore the behaviour of chains of qubits due to biologically-inspired qubit interactions and integrate the full synaptic theory of working memory into the quantum model. By analysing a three qubit-chain we show that it is possible to dynamically modify the period of a chain of qubits originally set up for perfect-state-transfer, and vary it over orders of magnitudes by using the interplay between "depression" and "facilitation". This translates into an interplay of state localisation and delocalisation. We also track quantum correlations' dynamics via two different types of entanglement. With single-site entanglement, we investigate how information flow across the chain is supported or impaired by the dynamics induced by the biologically-inspired interactions; qubit-to-qubit entanglement will be used to help shed light on the transfer of information between the chain's ends, as well as the possibility of creating and/or freezing useful entanglement. We also expand the 3 qubits system to a chain on N qubits with some preliminary results introduced in this thesis.

The results demonstrate a novel method for either accelerating or decelerating quantum information transfer across a qubit chain, a very useful functionality in quantum computing and other quantum devices. The different extensions to the original 2-qubits spin model and the parallel with biological systems contribute to the exploration of the behaviour of more complex chains of qubits, and more in general to the understanding of quantum information systems.

Acknowledgements

My studies in Quantum Physics have been fascinating since they began in 2019 with my Diploma in Physics at UCL. However, this research Master at York taught me how to be more rigorous in various aspects, such as plotting results or working out what might seem like simple calculations that are often taken for granted in research papers. I have also enjoyed exploring the simulation aspects of quantum systems; this was all new to me.

I want to thank my supervisor, Professor Irene D'Amico, for all our productive meetings and for introducing me to that great pub in York (The Rose and Crown) during my time as a Master by Research student. Fortunately, there is still more to do, and I am starting a new chapter, soon to pursue a part-time PhD under her guidance, which will investigate further the concepts discussed in this thesis.

Declaration of Authorship

I, Xavier Laurent, declare that this thesis titled, "Qubit chains' emergent behaviour from biologically-inspired dynamics" and the work presented in it are my own. I confirm that:

- This work was done wholly while in candidature for a research degree at this University.

- Where I have consulted the published work of others, this is always clearly attributed.

- Where I have quoted from the work of others, the source is always given. With the exception of such quotations, this thesis is entirely my own work.

- Part of the work from this thesis will be sent for publication in the journal APL Quantum.

- I acknowledge that I received assistance from generative AI to proofread this work in line with the policy on acceptable assistance with assessment.

List of digital tools used for my work

https://www.overleaf.com (Latex)

https://mathpix.com/ (Latex)

https://www.drawio.com/ (Diagrams)

https://elicit.com/ (AI Literature search)

https://scholar.google.com/ (Literature search)

Claude and ChatGPT (Gen AI)

https://github.com/xavlolo/quantum (Code repository)

https://www.spyder-ide.org/ (Code simulation)

Chapter 1

Introduction

1.1 Motivation

I have always been interested in the workings of the human mind. To learn more I worked towards a PhD in experimental psychology, with a focus on the study of human memory. It provided me a good understanding of some cognitive processes and started a passion for neuroscience and computation. Additionally, from a young age I have been captivated by physics, particularly the quantum world. I now feel that I can merge my two interests in these fields and help to build connections with potential practical applications, such as in quantum technologies.

I want to emphasise that my focus does not lie in the exploration of the quantum brain hypothesis and the topic of consciousness [27], even though a recent study reveals that networks of tryptophan (Trp), an aromatic amino acid integral to the construction of neurons, have been found to support robust quantum states in protein aggregates [7]. This is also an area worth investigating further. Instead, I am eager to investigate how the knowledge I have acquired from studying the brain and neuroscience (Fig. 1.1), can be applied to various quantum systems as represented in Fig. 1.2.

One promising research avenue that has been suggested to me at the start of my Master by my supervisor is the study of chains of qubits or "spin chains" and their diverse properties. I am particularly intrigued by the potential for incorporating neuronal properties into these systems and the implications this may have for quantum information processing. By bridging the gap between neuroscience, computation, and quantum physics, I hope to contribute some knowledge to these fields and see how this could lead to practical applications or be tested in a laboratory setting.

1.2 Outline

This thesis is divided into 4 main chapters. Chapter 1 describes the general background necessary to understand my work, covering aspects of biophysics and quan-
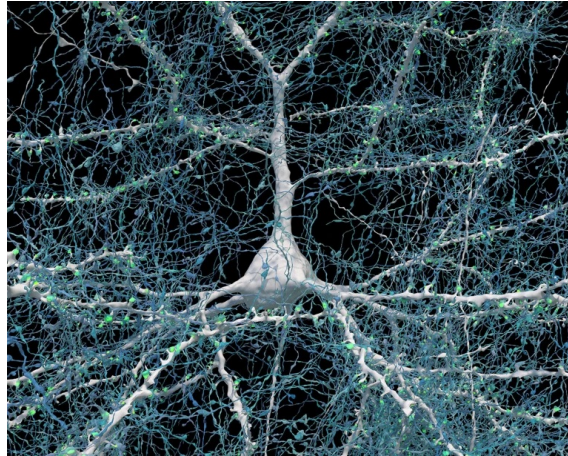
Figure 1.1: A single neuron (white) shown with 5,600 of the axons (blue) that connect to it. The synapses that make these connections are shown in green.Credit: Google Research and Lichtman Lab (Harvard University). Renderings by D. Berger (Harvard University)
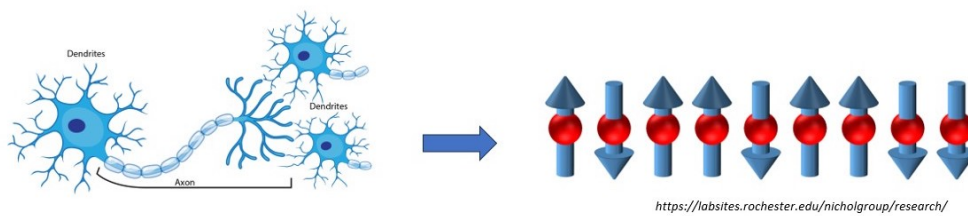
Figure 1.2: Neurons (left) and spin chain of qubits (right)

tum spin chains and their applications. Chapter 2 looks deeper into analytical content, for example, the working memory model, spin chains, perfect state transfer and entanglement. Chapter 3 illustrates how we have replicated the study conducted by Torres and Manzano[68]. This replication work helped me to build the foundation for my own research. Chapter 4 discusses the contributions we added to their model, which is the subject of a paper that we will submit to the APL Quantum Journal. Finally, we mark the beginning of an implementation for a spin chain of N qubits with preliminary results.

1.3 Biophysics

To contextualise the main theme of this thesis, I would like to explain why ideas from Working Memory (WM) models are relevant, why a specific type of WM model has been chosen, and how it will later be applied to the quantum domain.

1.3.1 Working memory definition

Working memory is the cognitive system that allows us to retain and manipulate information over short periods of time [22]. It is considered a fundamental cognitive process and is essential for a wide range of tasks, such as language comprehension, learning, and reasoning.

The synaptic theory of working memory [48] proposes that this temporary storage of information is accomplished through changes in the synaptic strength between neurons. This is in contrast to older models [34] of working memory that suggest that it is accomplished through persistent neuronal activity, see Fig. 1.3.

Figure 1.3: Neuron spikes or transient electrical impulses are represented by vertical lines. The retrieval cue serves to facilitate the recall. Fuster's experimental study [34] provided important insights into the role of Prefrontal Cortex (PFC) neurons in maintaining working memory across delays. However, the model did not directly explain the mechanism behind the disrupted firing during the random gap periods (in red). Hence other WM neural circuit mechanisms have been proposed. Figure from [34].

Specifically, the synaptic theory suggests that the activation of a specific memory trace, such as an image or a word, triggers a temporary strengthening of the synapses between the neurons involved in that memory trace. This temporary synaptic strengthening allows the information to be retained for a short period of time, even after the initial neuronal activity has ceased. A key advantage of the synaptic theory is that it provides a mechanism for how working memory can be maintained even in the face of distractors or other interference. Since the information is stored in the synaptic weights, it is not easily disrupted by other neural activity. Importantly, temporary synaptic strengthening is not just a theoretical construct; it is supported by evidence from studies on synaptic plasticity, particularly in animal models and neural tissue samples. Although observing this directly in a working human brain is currently challenging, experimental research has shown that similar processes, such as short-term potentiation (STP) and long-term potentiation (LTP), can occur in real synapses [75].

The theory further suggests that the manipulation of information in working memory is accomplished through the activation of specific patterns of strengthened synapses. For example, one is asked to remember a list of words and then rearrange them in alphabetical order, this would involve first strengthening the synapses associated with each word (retention) and then activating them in a new pattern (manipulation).

This idea builds on Hebb's postulate - a theory in neuroscience which states that if neuron A persistently takes part in firing neuron B, the synapses from A to B are strengthened [49]. This strengthening of connections between neurons has been observed to occur in real biological systems at both the cellular and molecular levels [47].

For example, synaptic efficacy can be increased, which is measurable by an increase in the amplitude or frequency of postsynaptic potentials in neuron B following presynaptic inputs from neuron A. Or structural changes, for example, an increase in the number of receptor sites or the enlarging of the area of synaptic contact. Finally, biochemical changes can include an increase in the release of neurotransmitters. .Thus, the synaptic theory of working memory suggests that short-term memory can be held in the synapses themselves, rather than through persistent activity.

Finally, it is important to note that the synaptic theory of working memory is a relatively new theory and is still being researched.Experimental evidence supports this theory, but more research is needed to fully understand the complexities of working memory and the role of synaptic changes while other mechanisms are also proposed [64], [25].

1.3.2   Synaptic transmission

To provide more insight that will lead to a mathematical model, we shall explain more what is meant by synaptic transmission, as it is a key feature of the working memory model.

There are two general forms of synaptic plasticity, intrinsic and extrinsic. Intrin-
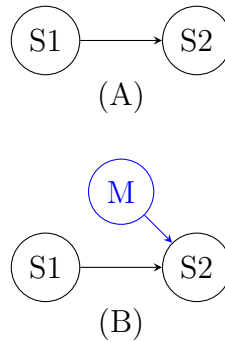
Figure 1.4: Illustration of homosynaptic mechanisms (A) and heterosynaptic (B) mechanisms. S and M depict neurons.

sic mechanisms, also known as homosynaptic mechanisms, refers to changes in the strength of a synapse that are brought about by its own activity, (Homo from the Greek meaning the same). Extrinsic plasticity, or heterosynaptic plasticity, is a change in the strength of a synapse brought about by activity in another pathway. For the thesis we are working with homosynaptic mechanisms (facilitation and depression), see Fig. 1.4.

Depending on the frequency of the stimulation at the pre-synapse the strength of the synapse can remain the same, weaker or stronger just by changing the frequency of activity. Networks of interconnected neurons operate will therefore depend on the level of activity within the circuit.

The transmission of the information encoded in firing patterns of the neurons is performed by the synapses to postsynaptic neurons through highly non-linear processes. These include, among others, the biophysical processes that control the trafficking and recycling of neurotransmitter molecules at the synapses and which are responsible for the transmission of the electrical signals among interconnected neurons.

To focus further there are two types of transmission. Short-term synaptic transmission allows for rapid modulation of neuronal communication, while long-term synaptic transmission mediates long-lasting changes in synaptic strength, enabling learning, memory formation, and neural plasticity. Here we are concerned with short-term synaptic transmission that occurs on a millisecond to minute timescale [75].

Synaptic transmission at a spike-mediated chemical synapse begins when an action potential from the presynaptic neuron invades the presynaptic terminal and activates voltage-dependent calcium (Ca2+) channels, leading to a rise in the concentration of Ca2+ within the terminal. The process is illustrated in Fig 1.5, this process leads to a mathematical model described in the chapter 2.
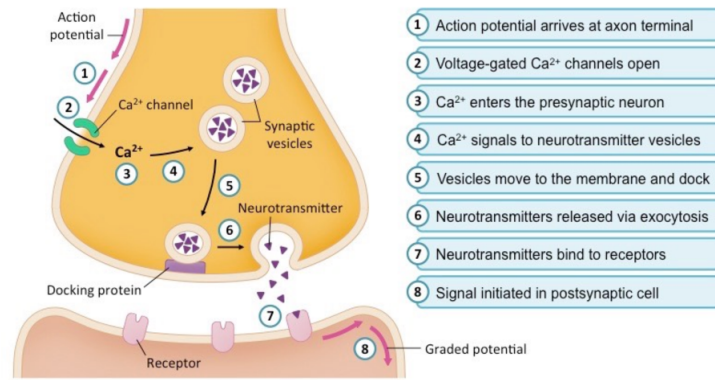
Figure 1.5: Visualisation of synaptic transmission from *Simply Psychology*, n.d.(https://www.simplypsychology.org/synapse.html)

1.4 Quantum spin chains

In this section we briefly review the concept of spin chain to help to make the jump between neuroscience and quantum systems. For detailed information on spin chains we would recommend the book *"Quantum State Transfer and Network Engineering"* [57], as in-depth review.

1.4.1 Spin chains

Spin chains, which are linear arrays of interacting quantum spins, stand as an important model for systems performing quantum information processing. These chains are renowned for their ability to smoothly transfer quantum information along their entire length, a key feature for quantum communication [13]. Additionally, Spin chains are instrumental in generating and distributing quantum entanglement[58], which plays an important role in quantum technologies [29].

Traditionally, gate-based systems often need complicated control, such as the toggling of connections between qubits. However, spin chains differ because of their operational simplicity and can bypass such requirements of qubit toggling. Spin chains can achieve this through the internal dynamics of the system, operating under the system natural Hamiltonian. This approach prevents errors from happening during frequent switching and reduces complications.

Physical implementations of quantum information processing are diverse, with each having unique characteristics and applications. Spin chains can be realized through various solid-state experimental platforms. For instance, quantum dots [46],[19], which are nanoscale semiconductor particles [23], or ions trapped in electromagnetic fields [16], can be viewed through the lens of spin chains. Other notable examples include superconducting qubits [8], used in quantum circuits, and optical waveguides [12], which guide light and can be coupled to function as quantum systems.
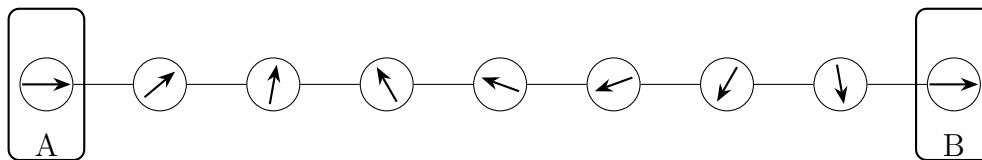
Figure 1.6: A general linear spin chain acting as a quantum bus between registers A and B. Here the circle represents the quantum spin, the segments between the circles represent the interactions. The transfer of a quantum state over a spin chain implies that the state that sits at one site is reliably transferred to another site of the chain.

1.4.2 Example of spin chains as quantum buses

Quantum computers, like their classical counterparts, require buses for data transfer without losing coherence. However, photonics presents challenges for short-range communication due to the need for conversion between solid-state qubits and light. Spin chains, originally proposed by Heisenberg [38], have been extensively reviewed in recent years, for example by Bose [13]. Others offer a promising alternative for quantum data buses by allowing data transfer with minimal external control and compatibility with solid-state qubits, mitigating the limitations of photon-based transmission [51].

The use of solid-state qubit chains as data buses hinges on the ability to transfer quantum states between sites with minimal external control. Various strategies focus on achieving what is called 'perfect state transfer' (PST) [45], exploring its effectiveness and examining the robustness of spin systems for the transfer of data. Fig. 1.6 is an example of a spin chain acting as bus between registers. More details are discussed in chapter 2 on PST and spin chain implementation.

1.5 Quantum systems with biologically-inspired qubits

Drawing inspiration from the field of neuroscience can significantly enrich quantum information research. In neuroscience, the modeling of neural systems often involves binary neurons with simplistic interactions between these units [67], which can be analogously represented by classical bits in a system. Yet, in classical neural networks and biological neural population models, an essential element emerges: the synapses. These are vital for the transmission of information encoded in the neurons' firing patterns. The process is highly nonlinear, involving complex biophysical processes like the trafficking and recycling of neurotransmitter molecules at the synapses, crucial for electrical signal transmission among interconnected neurons.

To conclude this overview, some literature on similar work where quantum design is inspired by neuroscience can be highlighted. Specifically chosen for survey are studies found most relevant to the thesis, assessing the current state of the field. The article by Torres and Manzano [68], which utilises dynamic synapses in the

implementation of 2 interconnected qubits and serves as an inspiration, is also presented in more detail during the mathematical model introduction and the study replication in Chapter 2 and 3, respectively.

A model of interacting quantum neurons with a dynamic synapse [68]

In this study, the authors investigate the behavior of quantum systems with qubit interactions inspired by neuroscience. Using a minimal model of two interacting qubits and activity-dependent dynamic interplay similar to classical dynamic synapses, they examine the effects of synaptic depression on the quantum system. Their findings show that without synaptic depression, the system exhibits typical Rabi oscillations, which decrease in frequency when synaptic depression is introduced, allowing excitations to be trapped for extended periods. The presence of synaptic depression also results in long-term entanglement between the qubits. The authors propose an experimental setup to validate these findings, suggesting that the results can be replicated in a laboratory setting. One of their motivations is to apply this work to Quantum Neural Networks (QNN)[1].

Additional noteworthy research in the intersection of quantum mechanics and neuroscience should be acknowledged:

Quantized single-ion-channel Hodgkin-Huxley model for quantum neurons [35]

The Hodgkin-Huxley model represents neuronal cell membrane behavior using electrical circuit elements. A simplified version of this model focuses on the potassium ion activation channel. By exploring a quantized Hodgkin-Huxley model based on quantum-memristor formalism, researchers compared membrane voltage and potassium-channel conductance behavior in both classical and quantum realms. The study found expected adaptations in channel conductance and discovered quantum features related to the circuit's zero-point energy. This research could enable the development of quantum neuron networks and neuromorphic quantum architectures for quantum machine learning applications.

An artificial neuron implemented on an actual quantum processor [67]

The study introduces a quantum information-based algorithm implementing a binary-valued perceptron for artificial neural networks, offering exponential advantage in storage resources. Researchers tested this model on a small-scale quantum processor, obtaining results consistent with expectations. The quantum perceptron can be trained using a hybrid quantum-classical scheme with a modified perceptron update rule, enabling it to classify simple patterns. This development serves as a first step towards practical quantum neural networks efficiently implemented on near-term quantum processing hardware.

An artificial spiking quantum neuron [42]

The study presents an artificial quantum spiking neuron that utilizes the dynamic evolution of two Hamiltonians and local measurements. This architecture takes advantage of complex amplitudes and measurement back-action to influence input, offering benefits when both input and output are quantum states. The approach is

demonstrated through the classification of Bell pairs. By stacking these elementary building blocks into larger networks, the spatiotemporal features of a spiking neural network are combined with non-local quantum correlations across the graph.

Modeling neuronal systems as an open quantum system [66]

A physical model is proposed to study neuron interactions by considering the materials surrounding neuronal cell bodies, such as dendrites, axons, synapses, and glial cells. This model is based on a continuous distribution of oscillating modes and uses the master equation approach from open quantum systems to analyze the dynamics. The model demonstrates the potential to generate random neuron-neuron interactions and may provide insights into the process of information transmission in the nervous system.

The papers reviewed represent an interdisciplinary effort to bridge classical neuroscience models with quantum mechanics. A central theme is the exploration of quantum mechanical counterparts or implementations of classical models, such as the Hodgkin-Huxley model, perceptrons, and spiking neural networks. This allows researchers to investigate the potential advantages and unique features that the modeling of neuronal systems and neural networks could offer for quantum systems. While some studies propose theoretical models, there is also a push towards experimentally validating these quantum neuronal systems and demonstrating their practical implementation, including testing on actual quantum processors [67], and exploring hybrid quantum-classical training schemes. Additionally, at least one study explores modeling neuronal systems as open quantum systems [66], taking into account interactions with the surrounding environment, aiming to capture the dynamics of information transmission in the nervous system from a quantum perspective.

Chapter 2

Mathematical models

2.1 Synaptic theory - facilitation and depression

This section discusses a minimal phenomenological model developed to mathematically represent the synaptic processes of depression and facilitation within the same synapse. There is also a simpler model, still based on the same approach, where depression or facilitation are described separately [2].

The phenomena of facilitation and depression in the synapses helps to understand the working memory model discussed previously and how short-term memories can be maintained without persistent activity.

Fig.2.1 depicts different types of synapses in the prefrontal cortex of a mouse. Some exhibit fast weakening or synaptic depression (E2a), while others exhibit fast strengthening or synaptic facilitation (E1b). Most importantly for the depression, the progressive decrease in spike amplitudes during repeated stimulation, or facilitation, the progressive increase in spikes does not disappear immediately; after half a second, the synapse is regaining its ability to release neurotransmitters effectively fully or is only partially recovered in some instance (E3b). The timescale of single seconds is necessary for working memory and his represented on the x axis.

For example, if there is a certain burst of activity in the neuron, even if it terminates for a certain time, the synapse still carries the information about the event. When the synapse is probed at a later stage after a new spike at the presynaptic neuron arrives, the information persists. For the information to disappear, one will need to wait a longer time.

The seminal paper [48] presents a simple phenomenological model based on these biophysical principles which fits the evoked postsynaptic responses observed on cortical neurons.

The mathematical model includes two kinetic processes for the same synapse, one responsible for depression (shown in blue) and another for facilitation (shown in red), sketched in Fig. 2.2. Depression is mediated by the release of neurotransmitters, while facilitation is physically mediated by the influx of calcium into the presynaptic
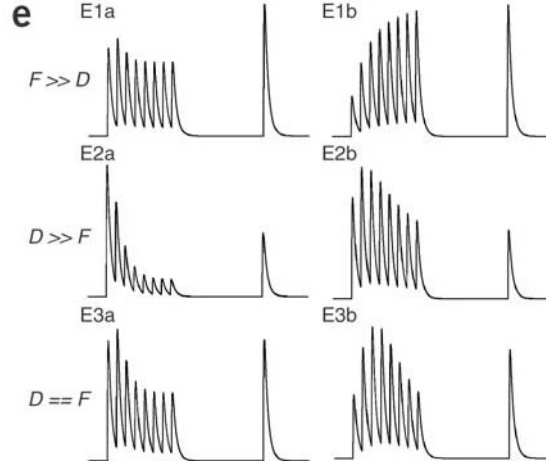
Figure 2.1: Post-synaptic responses in the cortical neurons of a mouse to a high frequency pulse of action potentials in the presynaptic neurons. On the x axis is time. Figure from [72].

terminal. These processes are described by their respective kinetic equations, with time constants for synaptic facilitation and depression as key parameters. By manipulating these parameters, the model can reproduce the rich synaptic processes observed in the brain as depicted in Fig. 2.1.

The synaptic facilitation process is modeled using the dynamic variable u (if $u = U$ is constant we would only have depression). The release probability of neurotransmitters is increased by the influx of calcium ions into the presynaptic terminal during a spike, see processes in Fig. 1.5. The dynamic variable u represents the instantaneous release probability, which increases with calcium influx and then decays over time with a characteristic time τ_f. Here, U represents the baseline release probability.

The synaptic depression process is modeled using the dynamic variable r. When a presynaptic neuron fires a spike, a fraction u of the available neurotransmitter is released. After release, the neurotransmitter resources are depleted, and they recover over time with a characteristic time τ_d, this corresponds to the processes in Fig. 1.5.

These two competing processes, depression and facilitation, can be adjusted by manipulating the time constants τ_d and τ_f, which influence the behavior of synapses according to

$$\frac{dr}{dt} = \frac{1 - r}{\tau_d} - ur\delta(t - t_{sp}) \tag{2.1}$$

$$\frac{du}{dt} = \frac{U - u}{\tau_f} + U(1 - u)\delta(t - t_{sp}) \tag{2.2}$$

By solving these equations for r and u, the model can reproduce the richness of synaptic processes observed in the brain, such as retrieving memory when the model is part of a neural network [48].

Appendix A provides a derivation of the equations used in this thesis from the original model presented in [37].
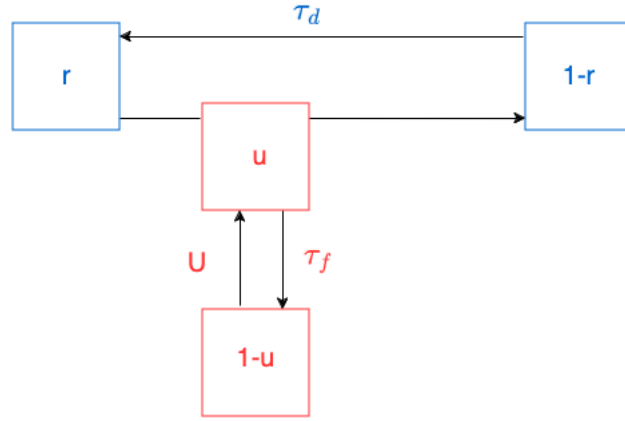
Figure 2.2: Kinetic scheme of the interplay between facilitation (blue) and depression (red). Here: τ_f (τ_d) is the facilitation (depression) characteristic time; u represents the instantaneous release probability (fraction of resources used after each spike) represented by the release of neurotransmitters process labeled 6 and 7 in Fig.1.5; r is the neurotransmitter recovery dynamics illustrated with 2,3,4,5 in Fig.1.5 and U is the baseline neurotransmitter release probability.

2.1.1   Summary of short-term synaptic plasticity

For a quick overview, the two competing processes of depression and facilitation are summarised in a table below.

Process	Description	Key Parameters	Role
Synaptic Depression	Guided by the release of neurotransmitters. Post-release, these neurotransmitters cannot be immediately replenished.	u (Neurotransmitter utilisation) τ_d (Time constant for depression)	Dictates the pace of neurotransmitter replenishment after release, and also acts as an indicator of the depression strength.
Synaptic Facilitation	Influenced by the calcium influx into the presynaptic terminal. A spike in the presynaptic neuron boosts the neurotransmitter release probability.	u (Neurotransmitter utilisation) τ_f (Time constant for facilitation)	Augments neurotransmitter usage rate, thereby amplifying the neurotransmitter release potential where elevated Ca2+ levels enhance the release of neurotransmitters. Regulates the decay rate of facilitation effects post-spike.

Table 2.1: Summary of synaptic depression and facilitation

2.2 Quantum spin chains - mathematical model

In this section we explain a few important concepts related to working with quantum mechanics and spin chains. These include descriptions of what is a spin, what a qubit represents, how to build an Hamiltonian, the concept of entanglement, and finally, perfect state transfer.

2.2.1 What is a spin?

Spin is a fundamental property of particles, like mass or charge. It describes the intrinsic angular momentum of a particle, which is a form of momentum that particles possess even when they are not moving in space. Unlike other types of angular momentum, spin does not have a classical analogue; it is a purely quantum mechanical phenomenon. The concept of spin applied to quantum mechanics was discovered in 1925 by two Dutch physicists, George Uhlenbeck and Samuel Goudsmit [14, p. 37].

Spin is quantized, meaning it can only take certain discrete values. For subatomic particles like electrons, protons, and neutrons, the spin is $\frac{1}{2}$ (in units of the reduced Planck's constant $\hbar$). This quantum number can take two projections along any axis: $+\frac{1}{2}$ or $-\frac{1}{2}$, commonly referred to as "spin up" and "spin down".

For enthusiasts of spin dynamics (rotation) in classical mechanics, there is a recently popular book (2023) titled "*The Science of Spin: The Force Behind Everything – From Falling Cats to Jet Engines*" that explores the scientific principles of spin [28]. Even more recently another new book (2024) "*The Wonder of Quantum Spin*" is more focused on the history and the science of quantum spin [62].

2.2.2 What is a qubit?

Bits serve as the fundamental units of information in classical computing, represented by any two-state device that can signify 0 or 1, positive or negative, true or false. In each case, a bit is well-defined to one of these two states. Drawing a parallel from biology, neurons function similarly, firing or not firing in a distinct binary pattern. However, diverging from this binary norm, quantum mechanics introduces the possibility for a two-level quantum system to exist in a state of superposition, a linear combination of its two potential states. This unique characteristic forms the basis of the qubit, the quantum computing counterpart to the classical bit. The term "qubit" itself is attributed to Benjamin Schumacher, who introduced it in 1995:

> "For our elementary coding system we choose the two level spin system, which we will call a 'quantum bit' or qubit. The qubit will be our fundamental unit of quantum information..." [63, p. 51].

In traditional digital computing, we define the two states of a bit as 0 and 1. Similarly, in quantum computing, the states of a qubit are represented as $|0\rangle$ and $|1\rangle$.

These states form what is known as the computational basis, consisting of orthonormal vectors. Any qubit can therefore be described by the equation

$$|\psi\rangle = \alpha|0\rangle + \beta|1\rangle, \tag{2.3}$$

where α and β are complex coefficients. The squared magnitudes of these coefficients, $|\alpha|^2$ and $|\beta|^2$, correspond to the probabilities of finding the qubit in the state $|0\rangle$ and $|1\rangle$, respectively. To ensure these probabilities correctly sum to one, the qubit state must always adhere to the normalization condition

$$|\alpha|^2 + |\beta|^2 = 1. \tag{2.4}$$

In quantum computing, the spin $\frac{1}{2}$ of particles can be used to represent qubits. There is a mathematical equivalence between a qubit and and a spin $\frac{1}{2}$. The two spin states $\left(+\frac{1}{2}\right)$ and $\left(-\frac{1}{2}\right)$ along a selected axis (often the z-axis in physics) can correspond to the qubit states $|0\rangle$ and $|1\rangle$. This makes physical spins, for example of electrons an excellent physical candidate for implementing qubits in quantum computers.

The computational basis is fundamental to quantum computing, serving as the primary framework for representing quantum states, performing calculations, and measuring qubits. To note that the basis in which one chooses to measure will depend on the physical system and the protocol one wish to implement. For example, in quantum algorithms, one might use the Bell basis or the Hadamard basis.

For a single qubit, we have chosen the following basis $|1\rangle = \begin{bmatrix} 0 \\ 1 \end{bmatrix}$ and $|0\rangle = \begin{bmatrix} 1 \\ 0 \end{bmatrix}$

Where $|1\rangle$ is associated with the "on" or one state, analogous to the classical bit value of 1 and $|0\rangle$ represents the "off" or zero state in quantum computations. It corresponds to the classical bit value of 0.

2.2.3 Quantum Hamiltonian

In quantum mechanics, the Hamiltonian H is an operator that encodes the total energy of a quantum system into its mathematical description. The Hamiltonian can include kinetic energy, potential energy, and interactions between particles within the system, depending on the complexity and nature of the system being studied [14, p. 85].

We consider in this thesis a linear spin chains with nearest-neighbor interactions, as described by the time-dependent XY-Hamiltonian

$$H_{XY} = \frac{1}{2} \sum_{i=1}^{N-1} \Omega_{i,i+1}(t) \left(\sigma_x^i \sigma_x^{i+1} + \sigma_y^i \sigma_y^{i+1} \right) + \sum_{i=1}^{N} \frac{\epsilon_i}{2} \left(\sigma_z^i + 1 \right), \tag{2.5}$$

where N is the total number of spins (qubits) and σ_x^i, σ_y^i, σ_z^i are the Pauli operators acting on spin i. With $\sigma_x = \begin{pmatrix} 0 & 1 \\ 1 & 0 \end{pmatrix}$; $\sigma_y = \begin{pmatrix} 0 & -i \\ i & 0 \end{pmatrix}$; $\sigma_z = \begin{pmatrix} 1 & 0 \\ 0 & -1 \end{pmatrix}$.

Here $\Omega_{i,i+1}$ is the interaction strength between nearby spins and it is time dependent. The second term on the right hand side represents the energy contributions from the z-components of the spins across the system, potentially under the influence of an external field or inherent material heterogeneity. The energy is time independent.

2.2.4 Entanglement

Entanglement stands out as the quintessential "non-classical" characteristic of quantum physics, laying the foundation for a host of innovative quantum applications. The first theoretical focus was discussed by Albert Einstein, Boris Podolsky, and Nathan Rosen, commonly referred to as the EPR paper in 1935:

> "Thus, by measuring either A or B we are in a position to predict with certainty, and without in any way disturbing the second system, either the value of the quantity P (that is p_k) or the value of the quantity Q (that is q_r)." [26, p. 780].

It acts as the essential component for teleportation [70], drives the functionality of measurement-based quantum processing and computing where entanglement serves as a resource [15], offers methods for secure communications [20], and enhances our sensing and measurement capabilities beyond the limitations of traditional instruments [32]. On a more entertaining note, entanglement is also depicted in science fiction programs, for example, in the recent (2023) Netflix hit "The Three-Body Problem", where an alien civilisation spies on humans using quantum entanglement [43].

When discussing entanglement in the context of quantum mechanics, another useful concept to introduce is the density matrix formalism. In principle, one can calculate everything in quantum mechanics using state vectors (pure states). However, there are some quantum experiments for which no single state vector can give a complete description (e.g. because of randomness or imperfections in experimental device). Hence a more useful formalism can help in these cases. This is called the density matrix or density operator formalism. Under this general description, any quantum system can be described. The formal definition is the sum of the projectors for each relevant pure state, weighted by their respective probabilities

$$\rho = \sum_{i=1}^{n} p_i \left| \psi_i \right\rangle \left\langle \psi_i \right|, \tag{2.6}$$

where p_i the classical probability of finding the system in the pure state $\left| \psi_i \right\rangle$ and with the fulfillment of the normalisation condition $\sum_j p_i = 1$.

In this thesis the overall state of the spin chain is a pure state. If the state of the quantum system is fully known the system is in a pure state ($\mathrm{tr}\left(\rho^2\right) = 1$). In our

case a bipartite pure state describes a system composed of two subsystems, A and B. A pure state of the combined system is represented by a vector $|\psi\rangle$ in the tensor product Hilbert space $\mathcal{H}_A \otimes \mathcal{H}_B$. The state is considered entangled if it cannot be written as a product of states of the individual subsystems.

We will regard negativity as an indicator of entanglement between ~~tow~~ two subsystems. For an n -qubit system represented by a density matrix ρ, the generalized negativity [71] $N(\rho)$ is defined as

$$N(\rho) = \frac{1}{2}\left(\sum_i |\lambda_i| - 1\right), \tag{2.7}$$

where, λ_i represent the eigenvalues of the partial transpose ρ^Γ of the density matrix ρ, with respect to one part of the system [56]. This could be any bipartite division of the n-qubit system into k qubits and $n - k$ qubits. A non-zero value of $N(\rho)$ indicates entanglement between the chosen partitions of the system.

Given a chain of qubits it is possible to consider different types of partition and hence compute different types of entanglement, two of which are detailed below.

Single site entanglement

In this type of bi-partite entanglement, the chain is partitioned into one qubit and the rest of the chain. When calculating the corresponding negativity for qubit Q, $N_{ss}^Q(\rho)$ from Eq. (2.7), the density matrix ρ will represents the whole qubit chain but ρ^Γ identifies the partition. This partition can be iterated along all qubits in the chain to observe how this entanglement changes across the chain. In a dynamical system, the time evolution of the single-site entanglement may help to understand the quantum correlation flow along the chain, related to the system state evolution and hence the flow of information.

This entanglement isolates the qubit to be analysed and look at the correlation with the rest of the qubits, as sketched for a chain of 3 qubits in Fig. 2.3.
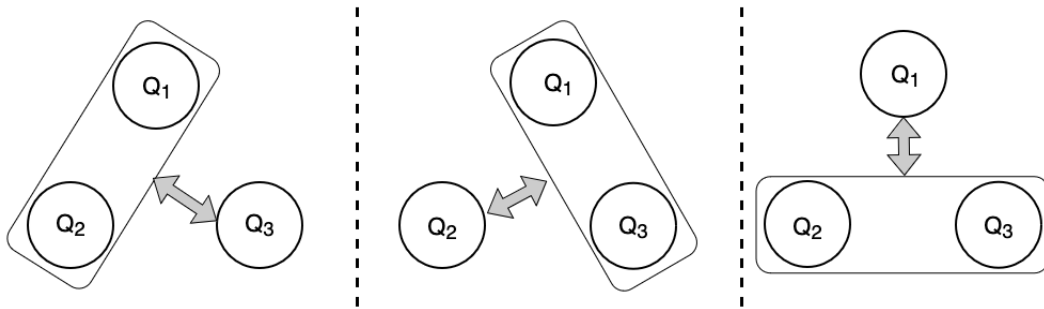
Figure 2.3: Bipartite splits for a single site entanglement between the three qubits Q_1, Q_2 and Q_3.

Qubit-qubit entanglement

Here the degrees of freedome of all qubits except two are traced out. The negativity $N_{qq}(\rho)$ between the two remaining qubits is then calculated from Eq.(2.7) using the

reduced density matrix. In this thesis, we will consider the entanglement between the two qubits at opposite ends of the chain. This can indicate how the chain dynamics either facilitate or hinder the potential for information transfer between the chain's extremities. Understanding these dynamics can be used for the optimisation of short-distance quantum communication protocols [73], creating and/or freezing useful entanglement [24], two-qubit gating [17], and to enhance the reliability and efficiency of quantum networks [29]-[59].

2.2.5   Perfect State Transfer

Another key concept explored in this thesis is Perfect State Transfer (PST).

Spin chains and networks hold promise as quantum data buses, but uniform coupling schemes have scalability limitations for example decay of fidelity (see e.g. [31]). To address this, various spin chain designs have been developed that enable efficient state transport over any chain length [6]-[29]-[59]-[30]-[5]-[53]-[45]-[52]-[18]. When these designs achieve perfect state transfer, meaning the transfer fidelity is perfect, they are particularly effective [41]-[4]-[50]. Fidelity is a way for measuring the proximity between states and is critical for understanding how successfully quantum information is transmitted [9]. It calculates the overlap of an evolved initial state $|\psi(0)\rangle$ with a desirable state $|\psi_{\mathrm{des}}\rangle$ at later time t [6] and is given for time independent Hamiltonian as

$$F(t) = \left| \left\langle \psi_{\mathrm{des}} \left| e^{-i\mathcal{H}t} \right| \psi(0) \right\rangle \right|^2. \tag{2.8}$$

PST is achieved in a quantum system when a quantum state initially localised at one site A can be transferred with unit probability to another site B after a certain time t. Mathematically, this means that the transition amplitude between these two sites, denoted as $F_{AB}(t) = \left\langle \psi_{\mathrm{des}} \left| e^{-i\mathcal{H}t} \right| \psi(0) \right\rangle$, should have an absolute value of 1 at some time t, ensuring that the state initially at A is perfectly transferred to B without any loss of information.

High-fidelity quantum state transfer can be achieved through various engineered methods. These include applying local magnetic fields [44] or wave-packet encoding [53]. Additionally, one of the most effective approaches is engineering the interactions between spins to facilitate PST for example vary the coupling strengths between adjacent spins in the chain [21]-[41].

In this thesis fidelity is not computed and a more extensive overview can be found in other works [29]. Specifically, the paper [21], investigate the necessary condition for the problem in the case of graphs with mirror symmetry, and the limitations of transfer in chains with uniform couplings.
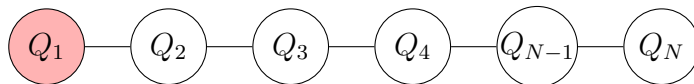
Figure 2.4: Six-qubits chain with excitation on Q_1.
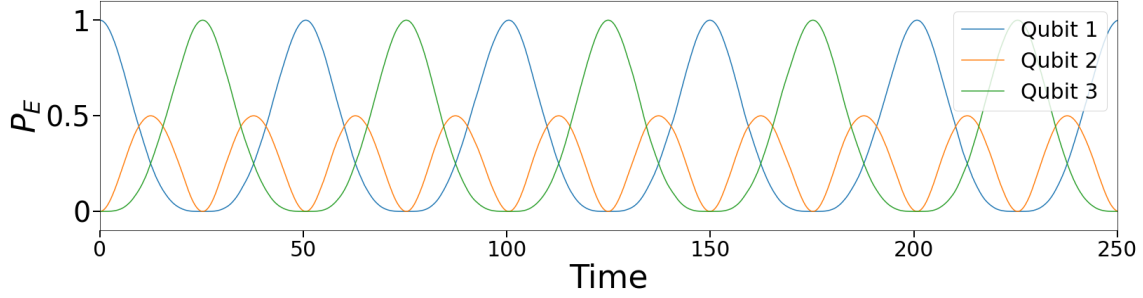
Figure 2.5: Occupation probabilities for the single site on the y axis (P_E) vs time for a spin-chain dynamics of 3 qubits. There is a perfect state transfer between Q_1 and Q_3. There is mirror symmetry, the graph is identical from the points of view of Q_1 and Q_3.

For uniform coupling it has been shown [21] that for $N = 2$ and $N = 3$ qubits, a perfect state transfer is achieved, but not for $N \geqslant 4$. To achieve perfect state transfer for $N \geqslant 4$, one must add a condition proposed in [21] and [50], where the $N - 1$ interactions of an N-sites linear chain are defined as

$$\Omega_{i,i+1} = \Omega_0 \sqrt{i(N-i)}, \tag{2.9}$$

with i being the site number. and $\Omega_0 = 2\Omega_{max}/N$ for even length chains and $\Omega_0 = 2\Omega_{max}/N \sqrt{1 - 1/N^2}$ for odd chains. Ω_{i+1} is the coupling value between nearby spins (energy).

In summary, the expressions for $F_{AB}(t)$ for $N = 2$ and $N = 3$ described in more details in [21] demonstrate PST because they can reach an absolute value of 1 at specific times, indicating that a quantum state can be transferred with unit probability across the chain. For larger chains ($N \geqslant 4$), achieving such precise conditions becomes increasingly difficult, leading to the conclusion that PST is not generally possible without certain conditions. In [21] the authors discussed the limitations for perfect communication of a uniformly coupled chain and proposed a proof by contradiction.

This PST condition can also be demonstrated with a simulation, see Fig. 2.5 with a spin chain for N=3 qubits. If the condition Eq. (2.9) is not implemented there is no perfect state transfer (Fig. 2.6), the fact that none of the curves remain consistently at 1 or 0 (indicating perfect transfer) suggests that there is no PST.
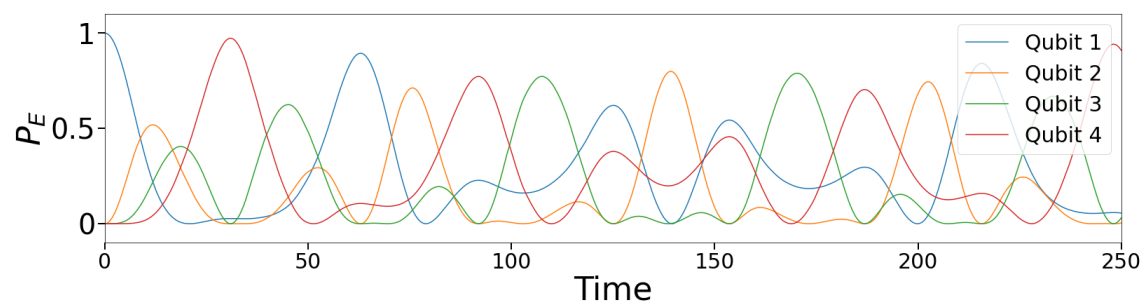
Figure 2.6: Occupation probabilities P_E for a spin-chain dynamics of 4 qubits. It can be noticed that there is no perfect state transfer between Q_1 (blue) and Q_4 (red), the condition for PST described in Eq. (2.9) is not implemented in this case.

Chapter 3

Replication of Torres and Manzano's results

3.1 Introduction

This chapter discusses how we reproduced relevant results in the paper of Torres, J.J., Manzano, D.: A model of interacting quantum neurons with a dynamic synapse. New J. Phys. 24, 073007 (2022).

Inspired by neuroscience, their work investigates the emergent behavior of quantum systems with biologically-inspired qubit interactions. Using a minimal model of two interacting qubits with activity-dependent dynamics similar to classical synaptic depression, they observe that without synaptic depression, the system shows typical Rabi oscillations. However, when introducing synaptic depression the oscillation frequency is reduced, allowing excitations to be trapped for extended periods and creating a population imbalance between the qubits. This imbalance is sustained by a small energy shift, that leads to long-term entanglement between the qubits. They also propose an experimental setup, suggesting that the findings are achievable in a laboratory [68]. Their results do not include synaptic facilitation, which is a key component of the synaptic theory of working memory described earlier.

3.2 Preliminary results

The first task for this thesis was to replicate the previous study before progressing to a more complex quantum system. This required learning the analytical and computational aspects of spin chains. Specifically, the initial work was to write a small program to solve the dynamics of an excitation in a trimer (a 3-site chain). This involved solving the time evolution of the system governed by the time-dependent Schrödinger equation, with a focus on using temporal discretization (Euler method) for time-integration.

This initial step helped in learning and reacquainting with coding and quantum

physics. Results from the small exercise were replicated using the Runge-Kutta methods, a family of iterative methods used for the approximate solution of ordinary differential equations. The fourth-order method (RK4) is most commonly used due to its good balance between accuracy and computational intensity.

The next step of the journey was to attempt to model a 2-qubit system to compute the excitation probability of a qubit using the same formalism, as Torres and Manzano's paper. To do so the evolution of the density matrix was tracked, specifically the diagonal elements which represent the probability of the system being in each of the site basis states. For example, $\rho(t)$ is obtained through numerical integration (using the Runge-Kutta 4th order method) of the system's dynamics, governed by the Liouville-von Neumann equation.

Finally, the qubit dynamics were integrated into the system with depression only, using the same paramter values as in the paper.

3.3 Methods

Based on the descriptions in the quantum, section 2.2, and the synaptic theory, section 2.1, the same Hamiltonian Eq. 4.1 was used with an added time dependency for the interaction strength between the two-qubits.
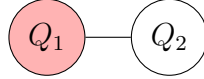
Figure 3.1: Sketch of a 2 qubits chain with single-qubit excitation on the first qubit (pink shade). This is the initial state.

Let's first examine the following time independent Hamiltonian for two non-interacting qubits without on-site energy contribution

$$H = \frac{1}{2}\Omega_{12}\left(\sigma_x^1\sigma_x^2 + \sigma_y^1\sigma_y^2\right). \tag{3.1}$$

One can rewrite the Hamiltonian in a matrix notation, that will be used later for computational purpose.

Consider the following expressions for the Pauli matrices

$$\sigma_x = \begin{pmatrix} 0 & 1 \\ 1 & 0 \end{pmatrix}; \; \sigma_y = \begin{pmatrix} 0 & -i \\ i & 0 \end{pmatrix}; \; \sigma_z = \begin{pmatrix} 1 & 0 \\ 0 & -1 \end{pmatrix};$$

Then, from Eq. (3.1) we have

$$H = \frac{1}{2}\Omega_{12}\left[\begin{pmatrix} 0 & 1 \\ 1 & 0 \end{pmatrix} \otimes \begin{pmatrix} 0 & 1 \\ 1 & 0 \end{pmatrix} + \begin{pmatrix} 0 & -i \\ i & 0 \end{pmatrix} \otimes \begin{pmatrix} 0 & -i \\ i & 0 \end{pmatrix}\right] \tag{3.2}$$

$$H = \frac{1}{2}\Omega_{12} \left[\begin{pmatrix} 0 & 0 & 0 & 1 \\ 0 & 0 & 1 & 0 \\ 0 & 1 & 0 & 0 \\ 1 & 0 & 0 & 0 \end{pmatrix} + \begin{pmatrix} 0 & 0 & 0 & -1 \\ 0 & 0 & 1 & 0 \\ 0 & 1 & 0 & 0 \\ -1 & 0 & 0 & 0 \end{pmatrix} \right]$$

$$H = \frac{1}{2}\Omega_{12} \begin{bmatrix} 0 & 0 & 0 & 0 \\ 0 & 0 & 2 & 0 \\ 0 & 2 & 0 & 0 \\ 0 & 0 & 0 & 0 \end{bmatrix} = \Omega_{12} \begin{bmatrix} 0 & 0 & 0 & 0 \\ 0 & 0 & 1 & 0 \\ 0 & 1 & 0 & 0 \\ 0 & 0 & 0 & 0 \end{bmatrix}. \tag{3.3}$$

In the paper [68] they considered the following Hamiltonian with adding the time dependency

$$H(t) = \epsilon_1\sigma_z^1 + \epsilon_2\sigma_z^2 + \frac{1}{2}\Omega_{12}r(t)\left(\sigma_x^1\sigma_x^2 + \sigma_y^1\sigma_y^2\right), \tag{3.4}$$

where the time dependency of the hopping parameter is related to the synaptic depression Eq. (2.1) as

$$\Omega_{i,i+1}(t) = \Omega_{i,i+1}r(t). \tag{3.5}$$

The time dependent Hamiltonian for symmetric and asymmetric case for 2 qubits can now be written as $\epsilon_1 = 0$ and $\epsilon_2 = 0$ and $\epsilon_1 = 0$ and $\epsilon_2 = 0.1$ respectively.

The Hamiltonian is symmetric with respect to the center of the chain (axis of symmetry) and has coupling with the same onsite energy, and it reads

$$H_1(t) = \begin{bmatrix} 0 & 0 & 0 & 0 \\ 0 & 0 & \Omega_{12}r(t) & 0 \\ 0 & \Omega_{12}r(t) & 0 & 0 \\ 0 & 0 & 0 & 0 \end{bmatrix}. \tag{3.6}$$

Asymmetry is represented by different onsite energy and symmetric coupling, that is

$$H_2(t) = \begin{bmatrix} 0 & 0 & 0 & 0 \\ 0 & 0.1 & \Omega_{12}r(t) & 0 \\ 0 & \Omega_{12}r(t) & -0.1 & 0 \\ 0 & 0 & 0 & 0 \end{bmatrix}. \tag{3.7}$$

Here $\Omega_{i,i+1}$ is the interaction strength between nearby spins, and $r(t)$ is the dynamic applied to the system in the context of depression, Eq. (2.1).

In [68] the authors are interested in how depression only may alter information transfer between the two qubits. A site-independent on-site energies with $\epsilon_i = 0$ can be regarded as the "perfect wire" for quantum data transmission. By randomising the value of onsite energy ϵ these type of chains are ideal for studying transport deterioration like Anderson localization [61].

3.3.1 Quantum version of the Tsodyks–Markram model: unitary dynamics

A quantum version of the Tsodyks–Markram model [48] is implemented, where depression $r(t)$ drive the time-dependent dynamics of the system Hamiltonian.

The equations determining the system dynamics are given by

$$\frac{\mathrm{d}\rho(t)}{\mathrm{d}t} = -i[H(t), \rho(t)] \tag{3.8}$$

$$\frac{\mathrm{d}r(t)}{\mathrm{d}t} = \frac{1 - r(t)}{\tau_d} - U r(t) \left\langle \sigma_1^+ \sigma_1^- \right\rangle (t) \tag{3.9}$$

Eq. (3.9) mimic the original classical model with the difference that the spikes in the depression dynamics are now driven by the population of qubit $1, \langle \sigma_1^+ \sigma_1^- \rangle$.

We consider a qubit to be 'excited' when it is in state $|1\rangle = \begin{bmatrix} 0 \\ 1 \end{bmatrix} = |\uparrow\rangle$. We then track the i-th qubit excitation probability using

$$P_{E,Qi} = \langle 1_i | \rho(t) | 1_i \rangle, \tag{3.10}$$

where $|1_i\rangle$ is a shorthand for a state with the i-th qubit in state $|1\rangle$, and all other qubits in state $|0\rangle = \begin{bmatrix} 1 \\ 0 \end{bmatrix} = |\downarrow\rangle$. The numerical integration of the system's dynamics is done using the Runge-Kutta 4th order method.

3.4 Results

In this section, the results of Torres and Manzano are presented using their original graphics, followed by the replication of occupation probabilities and entanglement. Our results closely align with their original findings.

The first two figures show the occupation probability. The first figure 3.2 presents the results from the paper, and the second figure 3.3 shows my simulation results.

The last two figures show the negativity. The figure 3.4 presents the results from the paper, and the second figure 3.5 shows my simulation results.

3.5 Discussion

In this study, only the results for occupation probability and negativity for both symmetric and asymmetric cases with the Hamiltonian described in Eq. (3.6) and Eq. (3.7) were reproduced. However, some mismatches were found. In certain instances, to achieve the appropriate results presented in the replication study, some
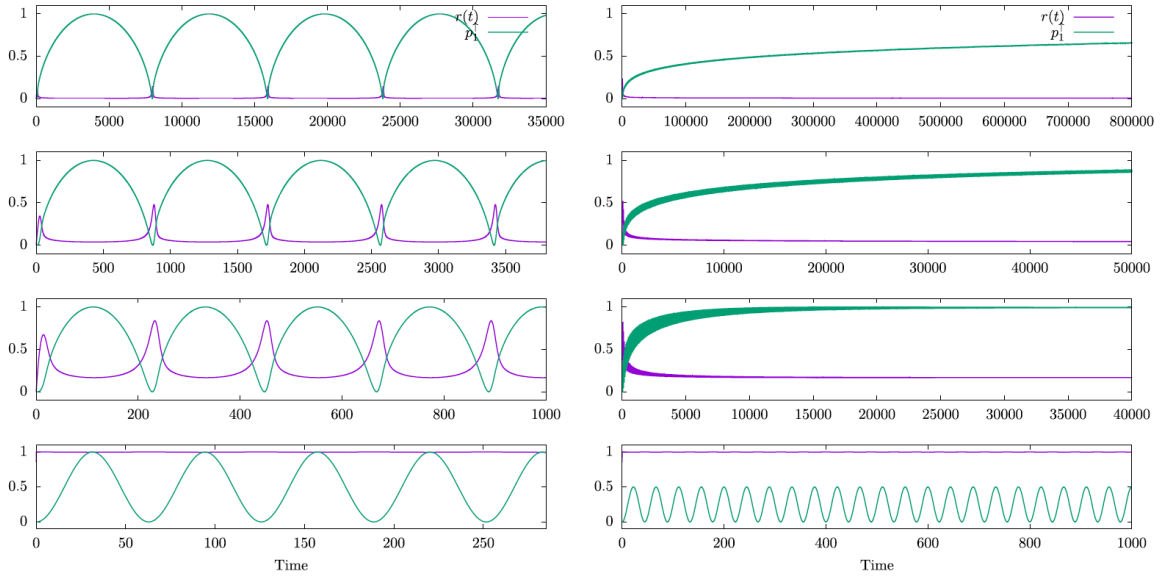
Figure 3.2: **Torres and Manzano's results for occupation probability**. Effect of dynamic synapses in an ideal two interacting qubits system. From top to bottom the level of synaptic depression in the system is decreased using, respectively, $\tau_d = 500, 100, 10, 0.001$. Other parameter values are $U = 0.5$, $\Omega = 0.05$. In the left panel it is shown the time dependence of the population (green line) of the first qubit as well as the Hamiltonian time-dependent parameter r(t) (purple line) for a symmetric system. In the right panel there is an on-site energy imbalance $\epsilon_1 = 0$ and $\epsilon_2 = 0.1$. Time given in natural units where $\hbar = c = 1$. Figures taken from [68], with permission granted by the author.
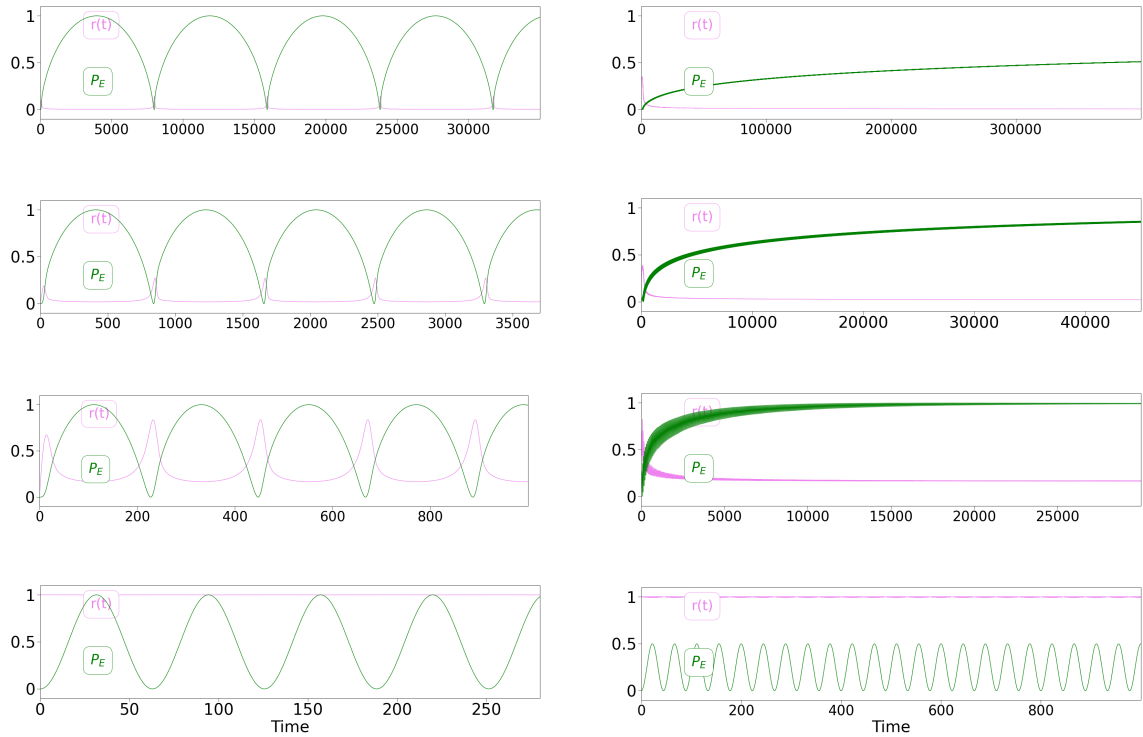
Figure 3.3: **Replication** of the effect of dynamic synapses in an ideal two interacting qubits system. From top to bottom the level of synaptic depression in the system is decreased using, respectively, $\tau_d = 500, 100, 10, 0.001$. Other parameter values are $U = 0.5$, $\Omega = 0.05$, $\delta t = 0.01$ and $\Omega = 0.1$ for $\tau_d = 100$. In the left panel it is shown the time dependence of the population (green line) of the first qubit as well as the Hamiltonian time-dependent parameter $r(t)$ (purple line) for a symmetric system. In the right panel there is an on-site energy imbalance $\epsilon_1 = 0$ and $\epsilon_2 = 0.1$, but for $\tau_d = 0.001$ we have set $\epsilon_2 = 0.05$.
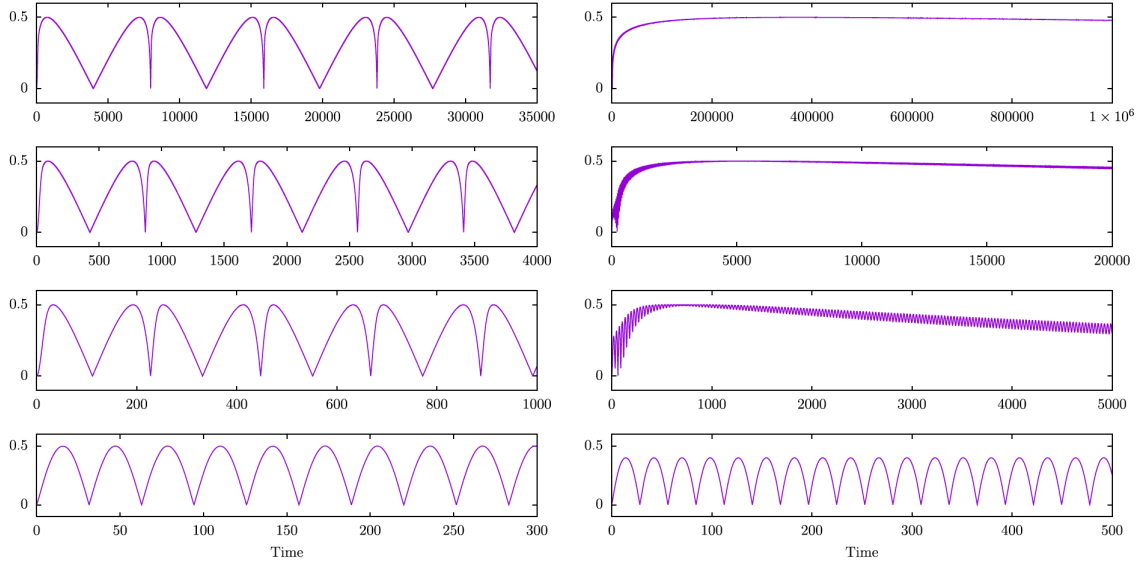
Figure 3.4: **Torres and Manzano's results for negativity:** Negativity of the systems as function of time. From top to bottom the level of synaptic depression in the system is decreased using, respectively, $\tau_d = 500, 100, 10, 0.001$. In the left panel it is shown for a symmetric Hamiltonian. In the right panel there is an on-site energy imbalance $\epsilon_1 = 0$ and $\epsilon_2 = 0.1$. Other parameter values are $U = 0.5$, $\Omega = 0.05$. Be aware of the different time scales of the plots. Figures taken from [68].

parameters had to be altered. Specifically, for both occupation probability and negativity, the value of Ω was changed to 0.1 for $\tau_d = 100$ in both symmetric and asymmetric cases.

One of the authors of [68] on February 4th, 2023, and May 2nd, 2024 was contacted, a response was received but there was no mention of the mismatches. Since this was not the main focus, the issue was not pursued further. Several checks on the computer code have been run and with the correct Hamiltonian, and no errors were found. We therefore decided to proceed to expand the study.
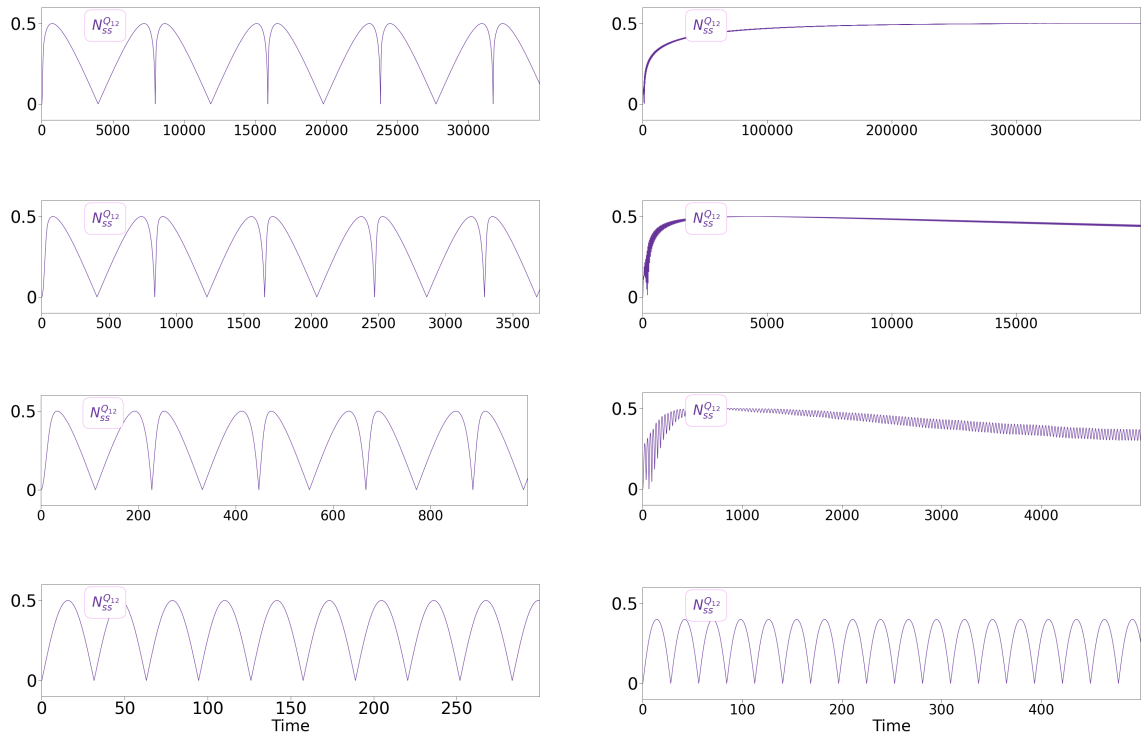
Figure 3.5: **Replication:** Negativity of the system as a function of time. From top to bottom the level of synaptic depression in the system is decreased using, respectively, $\tau_d = 500, 100, 10, 0.001$. In the left panel it is shown for a symmetric Hamiltonian for $\epsilon_1 = 0$, $\epsilon_2 = 0$. In the right panel there is an on-site energy imbalance $\epsilon_1 = 0$ and $\epsilon_2 = 0.1$. Other parameter values are $U = 0.5$, $\Omega = 0.05$ and $\Omega = 0.1$ for $\tau_d = 100$, $\delta t = 0.01$.

Chapter 4

Depression and facilitation in a longer spin chain

In this chapter, we first expand the model to a spin chain of three qubits. We further explore dynamics and entanglement for depression and symmetric cases. Importantly, we examine the impact of using the occupation probability of different qubits to drive non-linear dynamics and adding facilitation to the model. We present a cohesive series of results exploring the dynamics of a 3-qubit spin chain. Finally, we present preliminary results for chains of $N > 3$ qubits.

4.1   Hamiltonian for 3 qubits
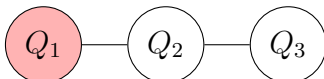
Figure 4.1: Three-qubits chain with excitation on Q_1 (pink shade).

We choose the XY model to describe the spin chain as

$$H_{XY} = \frac{1}{2} \sum_{i=1}^{N-1} \Omega_{i,i+1} r(t) \left(\sigma_x^i \sigma_x^{i+1} + \sigma_y^i \sigma_y^{i+1} \right), \tag{4.1}$$

where $\Omega_{i,i+1}$ is the interaction strength between nearby spins and $r(t)$ is the depression term.

Our focus first begins with the effect of depression dynamics, setting a baseline for subsequent analyses. We then extend our investigation to single-site entanglement within the chain, and further, to the entanglement between Q_1 and Q_3. Complementing this, we explore the impact of measurement in the sense explained in section 4.1.1 on the chain's dynamics.

Next, we present results on how the parameter U modulates these dynamics with

the depression and facilitation enabled , highlighting its critical role in shaping the quantum behaviour of the spin chain.

We then look at the interplay between depression and facilitation dynamics, and their collective contribution to the system's behaviour. Lastly we present preliminary results for chains with more than 3 qubits.

4.1.1 Quantum version of the Tsodyks–Markram model: non-linear feedback mechanism

We aim to enhance non-linearity in our approach while maintaining a unitary evolution. To this aim, we have merged the two approaches of Torres and Manzano as described below.

The equations we use now to determine the system dynamics are given by

$$\frac{\mathrm{d}\rho(t)}{\mathrm{d}t} = -i[H(t), \rho(t)] \tag{4.2}$$

$$\frac{\mathrm{d}r(t)}{\mathrm{d}t} = \frac{1 - r(t)}{\tau_d} - Ur(t)s(t) \tag{4.3}$$

Eq. (4.3) mimic the original classical model with the difference that the spikes in the depression dynamics are now driven by the stochastic variable s.

We implement a non-linear feedback mechanism which reacts to the flow of information across the chain in the quantum version of the Tsodyks–Markram model. In Ref. [68] two approaches are considered, a unitary evolution based on the average population of the second qubit, and a stochastic approach based on an actual measurement of that population followed by wave-function collapse. We choose to follow an intermediate method as explained below.

Like in the paper we use the stochastic variable s, which is updated at times $t_m = m\Delta t$ where $\Delta t = 0.01$ and depends on the local population of the i-th qubit in the chain as follows

$$s(t) = s_m \quad \text{for } t_m \leq t < t_{m+1} \tag{4.4}$$

with

$$s_m = \begin{cases} 1 & \text{if } x_{\mathrm{rand}} < \left\langle \sigma_i^+ \sigma_i^- \right\rangle \\ 0 & \text{if } x_{\mathrm{rand}} > \left\langle \sigma_i^+ \sigma_i^- \right\rangle \end{cases}, \tag{4.5}$$

and $x_{rand} \in [0, 1]$ is a random number from a uniform distribution.

The process in Eq. (4.5) mimics a measurement [68]. However, we do not collapse the wave function, as there is no necessity for this in a simulation. Instead the result is fed back through s to affect the dynamics of the depression variable $r(t)$. The idea is that the resulting simulation dynamics for $\Omega_{i,i+1}(t)$ can instead be stored and used to drive the related physical system in a lab. In this way the dynamics observed in our simulations could be obtained from a physical system in the lab.

Basically, the simulation can be employed to control a physical system. The benefits include not disturbing the physical system with measurements and avoiding the use

of an average over all possible dynamics given by imposing the collapse of the wave function. Perhaps it is apt to consider our simulation as a generator of chirped pulses' shapes to steer the physical system's dynamics.

4.2 Depression

In the first set of results we only include the effect of depression in the spin chain dynamics. To do so we use Eqs. (4.2) and (4.3) with U constant.

The results presented in Fig. 4.2 illustrate the impact of dynamic synapses on depression within a three-qubit chain. The figure shows an increasing level of synaptic depression from top to bottom, corresponding to $\tau_d = 0.01$, 10, 100 and 500, The other parameter values are set at $U = 0.5$ and $\Omega = 0.05$. The couplings are always the same they do not change with time. Each plot represents the probability of each qubit being in the $|1\rangle$ state (excitation probability, P_E) alongside the level of applied depression, represented by the $r(t)$ curve (blue curve).

It can be observed that the dynamics remain periodic across all levels of depression, even though the qubit-qubit coupling parameter undergoes significant dynamical changes within each period (as shown by the blue curve, for example in the second panel from the top). However, the period changes dramatically (by over two orders of magnitude), and the probability of finding at intermediate times, the excitation at one of the qubits at the end of the chain varies with τ_d.

The regime where this probability is high for a longer fraction of the period (low τ_d's) is referred as a 'localisation regime' (LR). This is where the first term on the rhs of Eq. (4.3) dominates. The opposite regime, where the wave function is spread across all three qubits for most of the time, is named as a 'delocalisation regime' (DR, high τ_d's). Here the second term on the rhs of Eq. (4.3) dominates. We will quantify and discuss further these regimes in the next sections.

4.3 Single site entanglement

The analysis covers LR: Localisation Regime and DR: Delocalisation Regime by examining the time evolution of single-site entanglement.

Fig.4.3 shows the negativity from Eq. (2.7) noted as $N_{ss}^{Q_i}(t)$ for $i = 1$, 2 and 3 (top, middle, and bottom panels respectively) for the DR dynamics shown in the bottom panel of Fig. 4.2 ($\tau_d=500$). Full localisation of the excitation in one qubit corresponds to zero negativity for all qubits. However, for the qubit experiencing full localisation, the corresponding negativity dip is very narrow, showing that the qubit very rapidly dis- and re-entangles with the rest of the chain. Notably, the almost-constant high value and very narrow dips in the negativity of Q_2 demonstrate that, in this regime, the wave function is almost always substantially delocalised over at least two qubits.
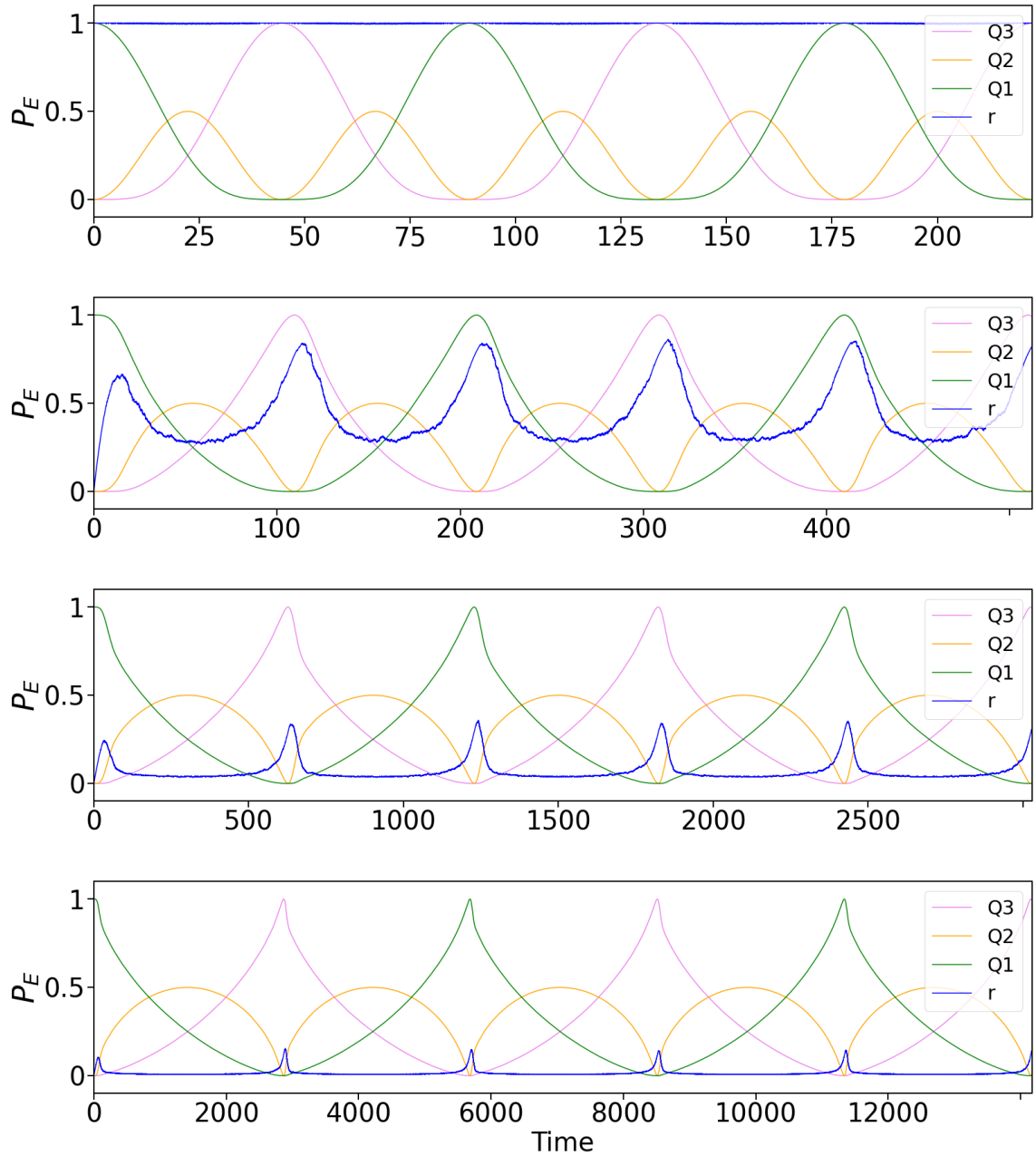
Figure 4.2: Excitation probability for Q_1 (green curve), Q_2 (orange curve) and Q_3 (violet curve) versus time. Blue curves track the dynamic depression coefficient $r(t)$. Initial state from top to bottom: $\tau_d = 0.01$, 10, 100, and 500. For all panels: $U = 0.5 = $ constant, $\delta t = 0.01$ and measurement taken on qubit Q_2. We plot 2.5 periods for Q_1.
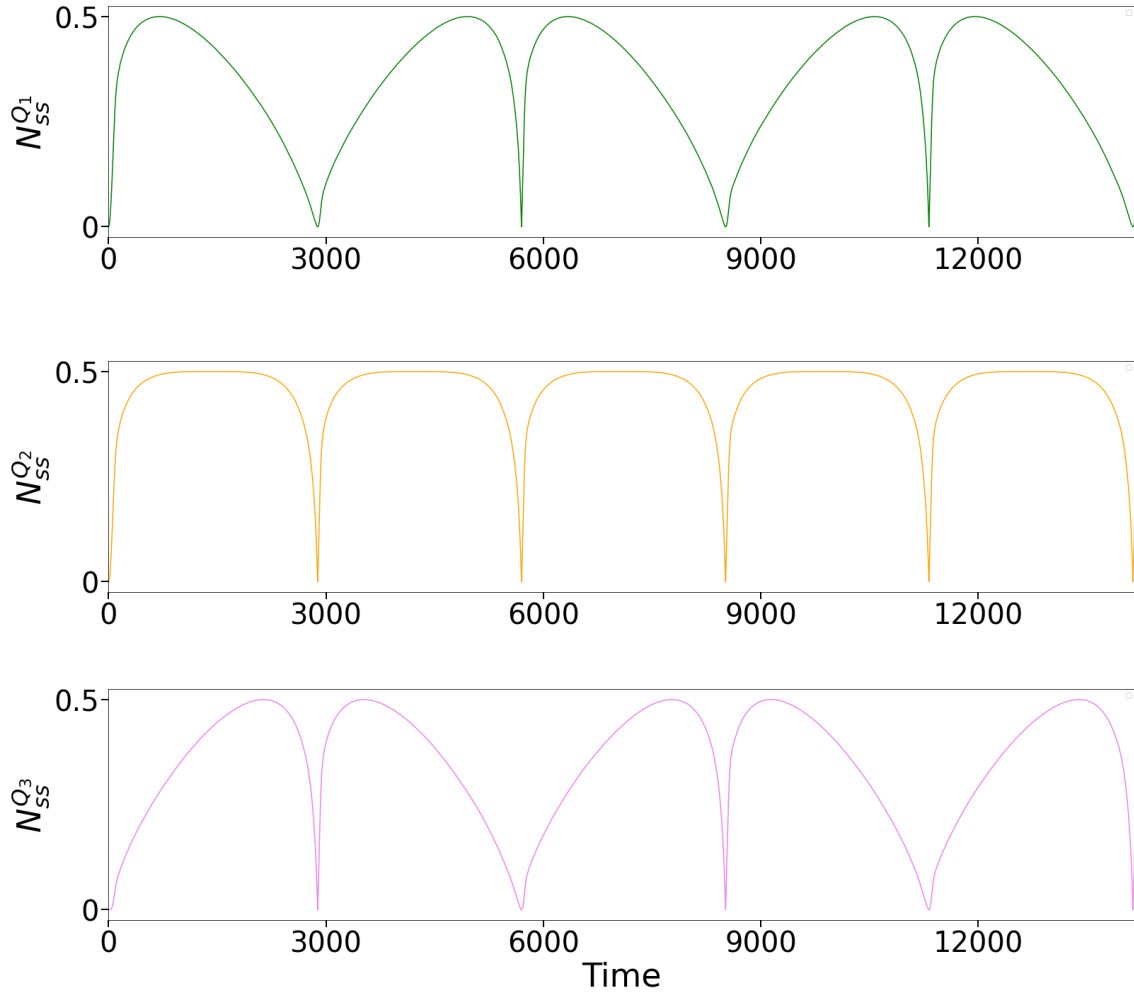
Figure 4.3: Single site entanglement: Negativity versus time for: top: Q_1; middle: Q_2; bottom: Q_3. For all panels: $U = 0.5$, $\tau_d = 500$, and measurement on Q_2.

This behaviour is qualitatively different from the corresponding 2-qubit case, where qubits show low entanglement over a relatively large fraction of the time period.

The single-site entanglement for the LR dynamics ($\tau_d = 0.01$) is illustrated in Fig. 4.4. It can be observed that, relative to the period length, the regions where all qubits are disentangled or have low entanglement are significantly wider than those in Fig. 4.3. For instance, compare the dips at $t \approx 45$ in Fig. 4.4 with those at $t \approx 3000$ in Fig. 4.3. This is more inline with the corresponding results for the 2-qubit chain, see Fig. 3.5.

4.4 Entanglement between end qubits

The study also focuses on the entanglement between qubits Q_1 and Q_3, which measures their direct quantum correlation, independent of Q_2's state.

The entanglement between Q_1 and Q_3 measures how much Q_1 and Q3 are directly
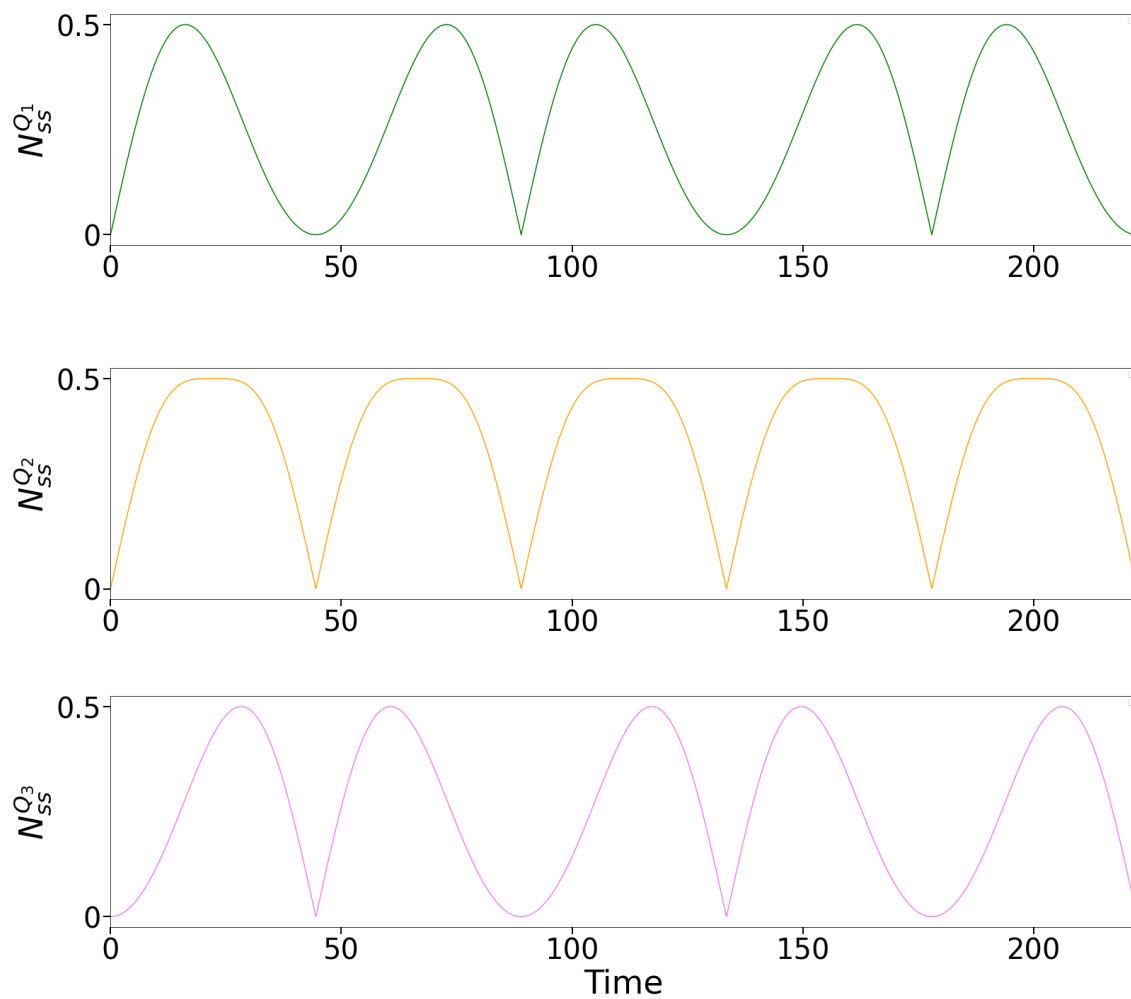
Figure 4.4: Single site entanglement: Negativity versus time for: top: Q_1; middle: Q_2; bottom: Q_3. For all panels: $U = 0.5$, $\tau_d = 0.01$, and measurement on Q_2.

correlated, i.e. how much they are (quantum) correlated independently from the value of Q_2.

We find that the dynamics of the entanglement as measured by the corresponding negativity, calculated from Eq. (2.7) is tied to to the occupation probability of Q_2 in Fig. 4.5. In both cases of low and high depression the negativity $N_{qq}^Q(\rho)$ for Q_1 and Q_3 has the same maximum at 0.1.

The entanglement between Q_1 and Q_3 is qualitatively similar to the single-site entanglement for Q_2 , but much smaller. For both cases of low and high depression: the shape reflects the symmetric role that Q_2 has with respect to Q_1 and Q_3 and the entanglement goes to zero when the excitation fully localises on one of the qubits (i.e. occupation of one of the qubits is equal to 1).

4.5   Effect of measurement location

How we choose the measurement location in our protocol is crucial for influencing the dynamics of the spin chain. Specifically, in a PST chain with static couplings as described in Eq. (2.9), and with three or more qubits, the excitation probability dynamics of the inner qubits differ qualitatively from those of the qubits at the ends of the chain. We will demonstrate how this can be utilised to switch between DR and LR and to significantly modify the period of the chain.

In Fig. 4.6 we compare the excitation probability dynamics of a 3-qubit chain when the feedback measurement in the protocol is done on Q_1 (upper panel), Q_2 (middle panel) and Q_3 (lower panel), with $\tau_d = 500$ (high depression rate). Measurement on Q_2 induces DR. However, without other changes in parameters, measurement in Q_1 (Q_3) localises the excitation on qubit Q_1 (Q_3) for most of the time, compare green (violet) curves in top (bottom) and middle panels. In addition, it increases the period by about 50%. We note that, in all cases, a periodic dynamics is maintained.

Without the need of adding facilitation to the Hamiltonian, feedback measurement on Q_3 facilitates excitation transfer to the chain end: the excitation probability in Q_3 rises above 50% at $t \approx 800$, compared to $t \approx 2000$ for the case of measurement done on Q_2 and $t \approx 4000$ for measurement done on Q_1. At the same time, by inducing LR on Q_3, feedback measurement on Q_3 improves conditions for measuring the excitation at Q_3 or for further transferring it (e.g. via SWAP gate) from there to a different quantum computational array. We note though that maximum probability on Q_3 is reached at the same time when measuring on Q_1 or on Q_3.

At the other extreme, without altering depression parameters, measurement on Q_1 strongly inhibits transfer by both localizing at most times the excitation in Q_1, and reducing by about 6 times the size of the intervals at which $P_{E,Q3} > 50\%$ with respect to when measurement is done on Q_2 (compare violet curves in top and middle panels), and by almost 30 times with respect to measurement on Q_3. We note that these effects are linked to the application of a significant depression.

By contrast, when we consider feedback measurement with negligible depression,
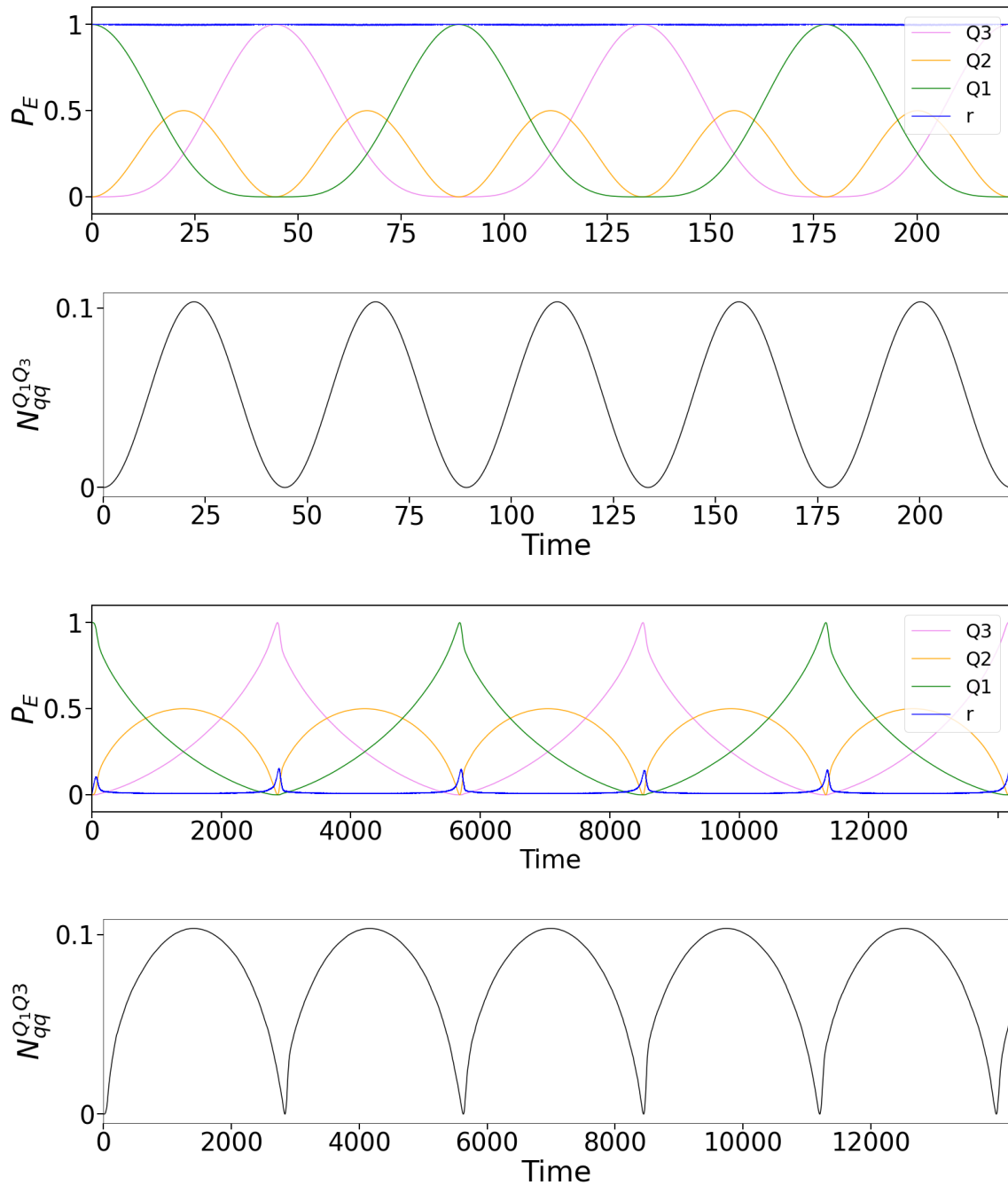
Figure 4.5: In black entanglement between qubits Q_1 and Q_3 with tracing of Q_2. Blue curve tracks the dynamics depression coefficient $r(t)$. Excitation probability for Q_1 (green curve), Q_2 (orange curve) and Q_3 (violet curve) From top to bottom: $\tau_d = 0.01$ (panels 1,2) and 500 (panels 3,4) . For all panels: $U = 0.5$, and measurement taken on Q_2. We plot 2.5 periods for Q_1.
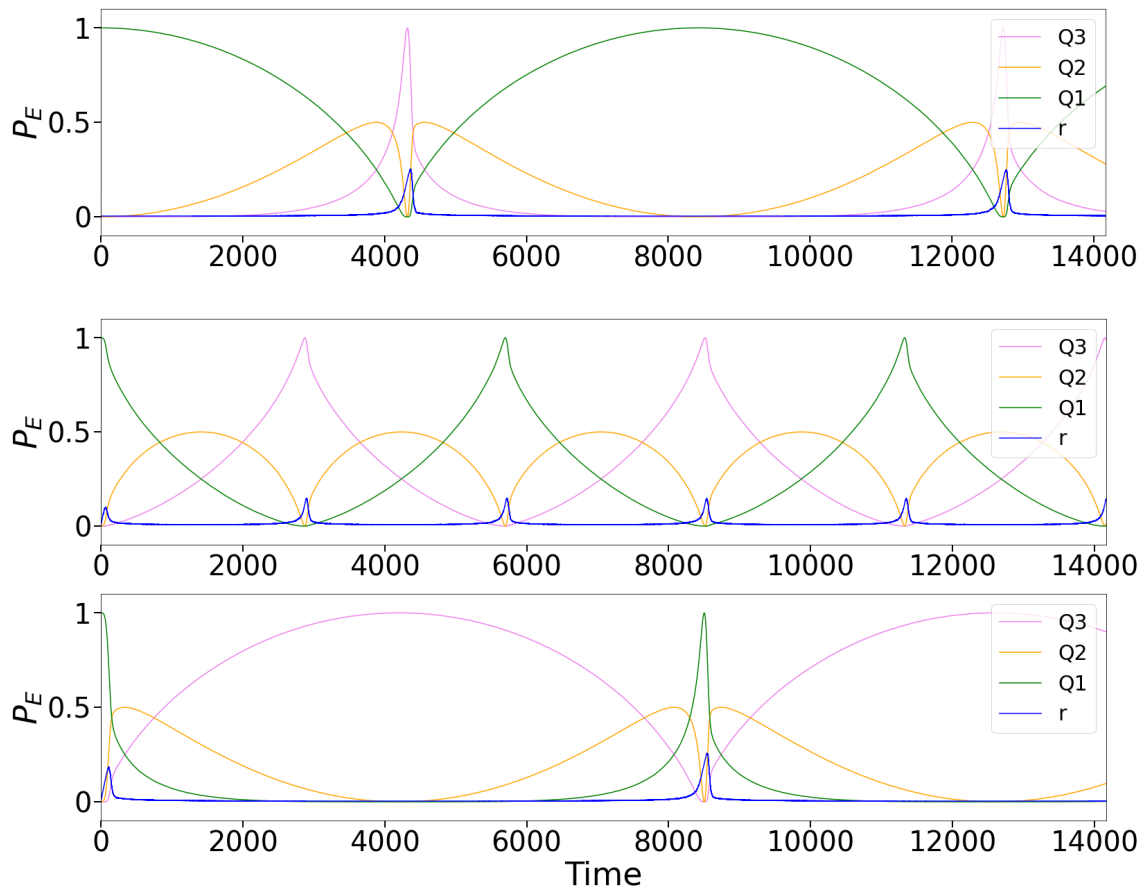
Figure 4.6: Excitation probabilities vs time for feedback measurement in different sites: Top: Q_1 (green); middle: Q_2 (yellow); Bottom: Q_3 (violet). For all panels: $U = 0.5$, $\tau_d = 500$, and $\delta t = 0.01$.
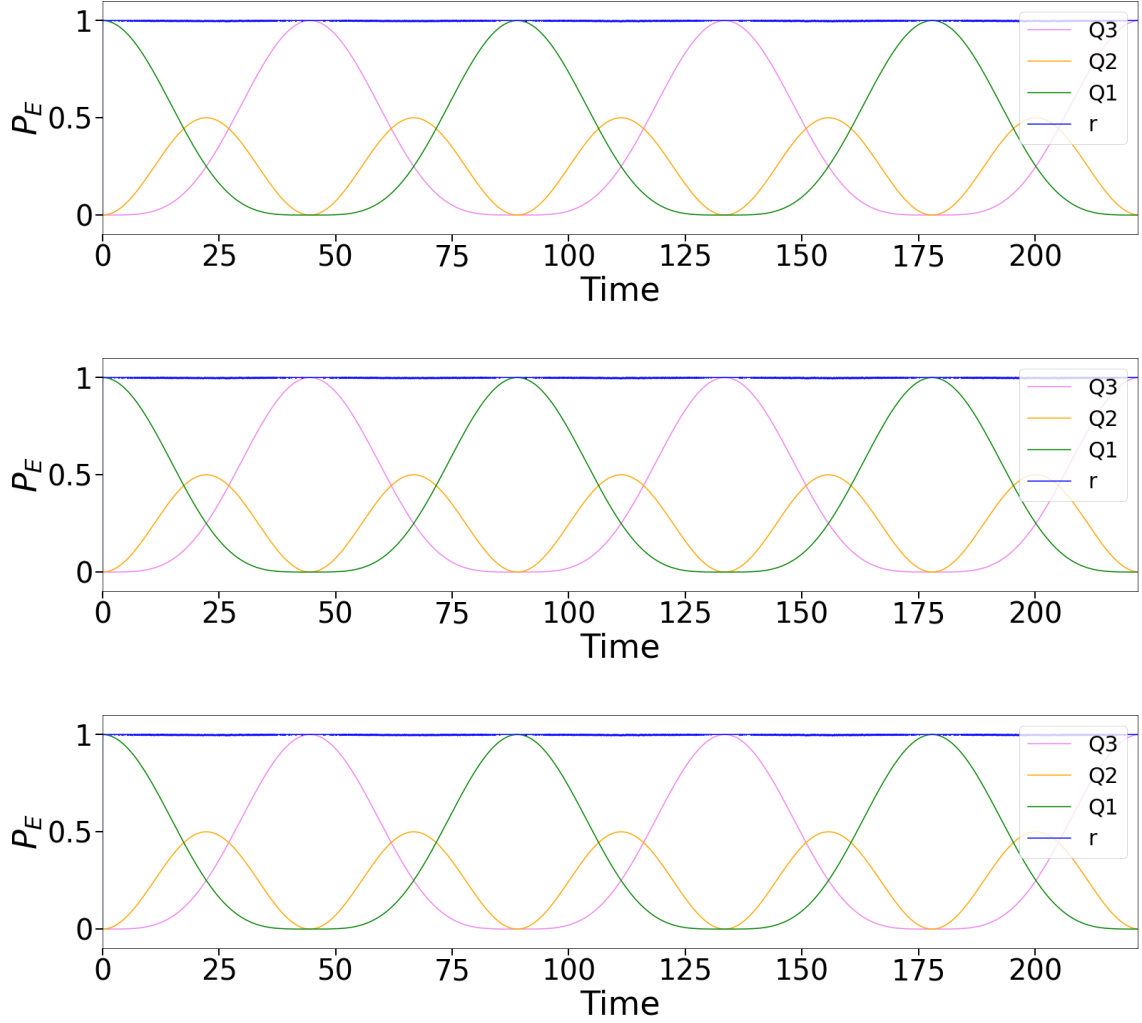
Figure 4.7: Excitation probabilities vs time for feedback measurement in different sites: Top: Q_1 (green); middle: Q_2 (orange); Bottom: Q_3 (violet). For all panels: $U = 0.5$, $\tau_d = 0.01$, and $\delta t = 0.01$.

$\tau_d = 0.01$, we observe no changes in the dynamics, see Fig. 4.7. In this case, the time evolution of $r(t)$ is in fact mainly due to the first term on the rhs of Eq. (4.3).

4.6   Impact of the release probability U on occupation probabilities

We also noticed that U can play a role in the dynamics of the system. For instance, the period's length tends to increase linearly with U, depending on the values of τ_d. This is plotted in Fig. 4.8 where on the Y axis is the Transfer time (T_{tr}) of information between Q_1 and Q_3.

The transfer time can be defined as

$$T_{tr} = t\left(P_{E,Q_3} = 1\right) - t\left(P_{E,Q_1} = 1\right). \tag{4.6}$$
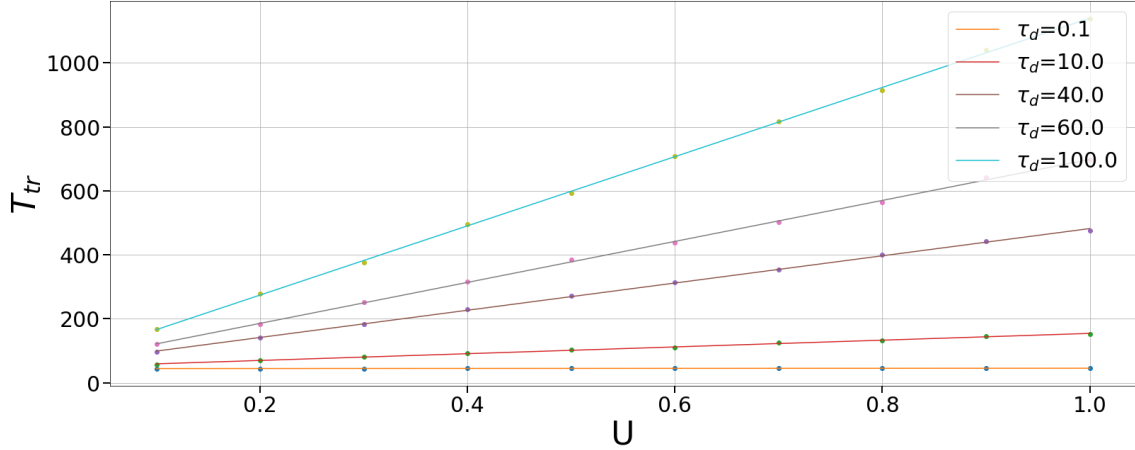
Figure 4.8: Effect of U: Time of transfer (T_{tr}) (averaged over 3 consecutive periods) for the expectation between Q_1 and Q_3 vs U for different τ_d with $\delta t = 0.01$.
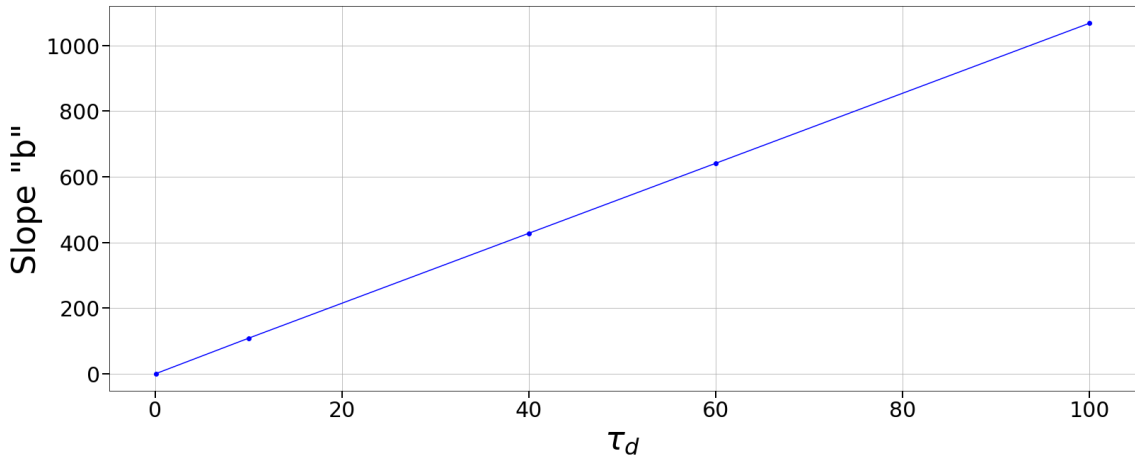
Figure 4.9: Coefficient b from $T_{tr} = a + bU$ for various τ_d with $\delta t = 0.01$.

In Fig. 4.8, each point corresponds to the average of difference of T_{tr} over the first 3 periods. Then, a least-squares polynomial fit of degree 1 (a straight line) method was used to fit the data, producing the straight lines. For small values of τ_d, the transfer time between Q_1 and Q_3 remains relatively constant. As τ_d increases, the transfer time starts to increase rapidly. It shows that large values of τ_d can lead to higher transfer times between the qubits.

The release probability U provides another means to control the system's periodicity. This interplay between U and the influence of different τ_d values in a three-qubit chain, either accelerates or decelerates communication across the spin chain, demonstrating a quantum effect.

In Fig. 4.9 we have plotted the slope (coefficient b), for different τ_d, of values $T_{tr} = a + bU$. The figure shows a linear relationship between τ_d and b.
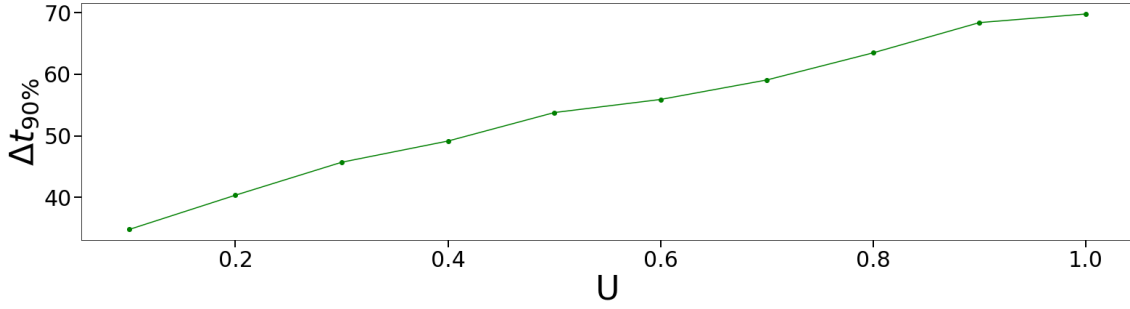
Figure 4.10: Average duration of high excitation intervals for Q_3 (where $P_{E,Q_3} \geq 0.9$) versus baseline utilisation factor U. Each data point represents the mean time duration during which $P_{E,Q_3} \geq 90\%$, averaged over the first 3 periods. The data is obtained under conditions of synaptic depression with a time constant $\tau_d = 100$, $\delta t = 0.01$.
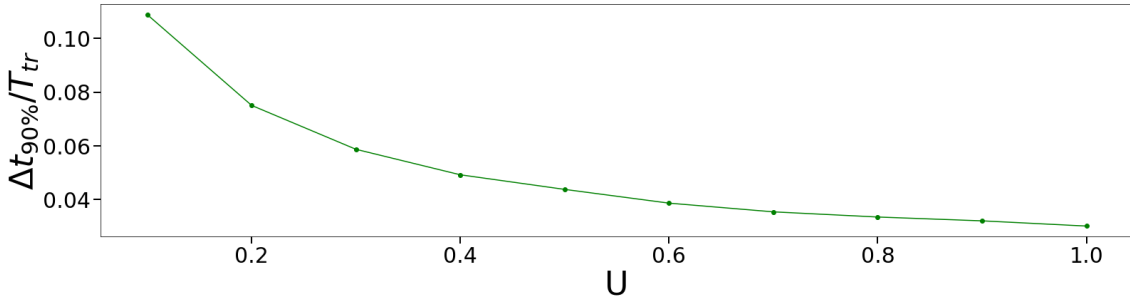
Figure 4.11: Normalised (divided by T_{tr}) average duration of high excitation intervals for Q_3 (where $P_{E,Q_3} \geq 0.9$) versus the baseline utilisation factor (U). The data is obtained under conditions of synaptic depression with a time constant $\tau_d = 100$. Each point represents the average over the simulation of the first 3 periods, with $\delta t = 0.01$.

4.6.1 Average duration of high excitation intervals and average fraction of time per period versus baseline utilisation factor

Fig. 4.10 shows the time $\Delta t_{90\%}$ in which we have at least 90% probability of measuring the excitation in Q_3 with respect to U. We can think of it as localisation time for that particular qubit, and it can be noticed that the time the excitation can be measured in Q_3 with 90% probability or more over a period is increasing with U.

In Fig. 4.11 we consider the average high excitation per transfer time $\Delta t_{90\%}/T_r$ with respect to U, this fraction decreases with U. By comparing results in Fig. 4.11 and 4.10, the fraction of the period spent in high excitation decreases, it suggests that while the high excitation states are lasting longer, the transfer time (from one peak to the next) is increasing at a faster rate.

A more intuitive way to visualise the data is to plot the occupation probability for P_{E,Q_3} versus time for different values of U, see Fig. 4.12. We can observe the following.
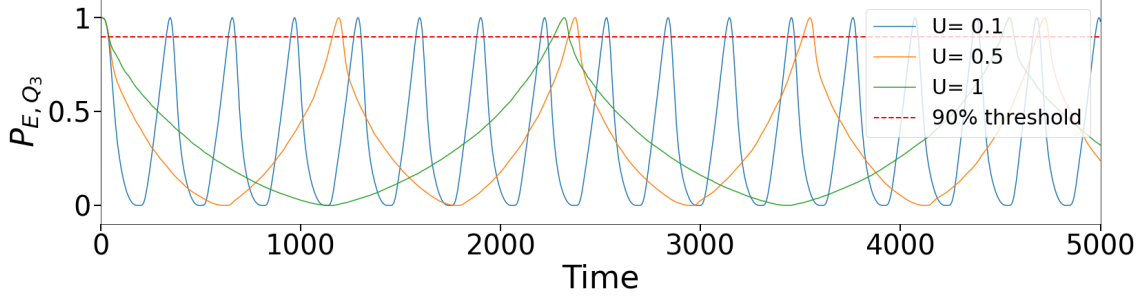
Figure 4.12: Occupation probability P_{E,Q_3} for Q_3 with $\tau_d = 100$ versus time and measurement on Q_2, $\delta t = 0.01$.

When examining the portion of the curve above the 90% mark (dashed curve) for a single period, the duration of the blue curve is shorter than that of the green curve ($U = 1$). Specifically, the time interval above the 90% mark for the green curve is approximately 1.5 times longer than that for the blue curve. However, for one period of the green curve, we observe seven periods for the blue curve.

For $U = 0.1$, the occupation probabilities oscillations are more frequent , i.e they have shorter periods. The peaks reach above the 90% threshold more often compared to higher U values. Despite the high frequency, each individual duration of time spent above the 90% threshold is short. However, over the whole simulation time, the high frequency compensates for the short duration above the threshold.

For $U = 1$, the oscillations are the least frequent and have the longest periods. The peaks above the 90% threshold are much less frequent compared to $U = 0.1$ and $U = 0.5$ (orange curve). However, the time interval spent above the 90% threshold in each oscillation is longer but not long enough to compensate over the reduced frequency when considering the whole simulation time.

4.7 Interplay of depression and facilitation

So far only depression was considered. When facilitation is added, the release probability varies with time and becomes $U = u(t)$. The new Hamiltonian is with the dependence of $\Omega_{i,i+1}(t)$ from the time discussed below.

$$H_{XY} = \frac{1}{2} \sum_{i=1}^{N-1} \Omega_{i,i+1}(t) \left(\sigma_x^i \sigma_x^{i+1} + \sigma_y^i \sigma_y^{i+1} \right). \tag{4.7}$$

The equations determining the system dynamics are now given by

$$\frac{\mathrm{d}\rho(t)}{\mathrm{d}t} = -i[H(t), \rho(t)], \tag{4.8}$$

$$\frac{\mathrm{d}r(t)}{\mathrm{d}t} = \frac{1 - r(t)}{\tau_d} - u(t)r(t)s(t), \tag{4.9}$$

$$\frac{\mathrm{d}u(t)}{\mathrm{d}t} = \frac{U - u(t)}{\tau_f} + U(1 - u(t))s(t). \tag{4.10}$$

We can now explore the form of $\Omega_{i,i+1}(t)$ when facilitation is included. The time dependence for the coupling could take various forms, such as $\Omega * r(t)$, $\Omega * u(t) * r(t)$, or $\Omega * (u(t) + r(t))$. It is important to note that we are still keeping both couplings the same at all times. According to the original classical model, the product of the two variables $u(t)$ and $r(t)$ should be considered.

However, for the quantum model, we have explored the various forms of coupling in out Hamiltonian and we only included $r(t)$ in $\Omega_{i,i+1}(t)$. Different tests were conducted to observe the impact of adding $u(t)$ explicitly as discussed below.

According to experimental reports from real neurons, facilitation for excitatory connections occurs when $\tau_f \gg \tau_d$, with τ_f on the order of 1.5 seconds and τ_d on the order of 0.2 seconds [48] (we did not used these exact values in the simulations). In the results we keept $U = 0.5$ and only varied the time constant for depression and facilitation.

The graphs Fig. 4.13 and Fig. 4.14, illustrate the occupation probability over time for different sets of parameters, specifically focusing on the variables $r(t)$ and $u(t)$.

In the plots in Fig. 4.13, we used a more realistic value of τ_f, following the values described in the Mongillo study [48]. It can be observed that there is little impact on the dynamics of the occupations. In the next set of plots Fig. 4.14, we increased the values of τ_f and τ_d to a greater extent. While the shape of the dynamics remains the same when increasing τ_f with respect to τ_d, there appears to be a slight impact on the periodicity of the occupation probability.

The next set of graphs in Fig. 4.15 shows the influence of how $u(t)$ is integrated into the Hamiltonian. So far, we have not included $u(t)$ in the coupling and have only considered $\Omega * r(t)$. Now, we present two separate graphs. The first graph is for $\Omega * u(t) \cdot r(t)$, and the second graph is for $\Omega * (u(t) + r(t))$. The dynamics remain the same, except that we have doubled the frequency.

If $u(t) = 1$, it would explain why with $r(t)$ or $r(t) * u(t)$ in the Hamiltonian we obtain the same dynamics. Adding $r(t) + u(t)$ in the Hamiltonian seems to double the frequency, so it would suggest $r(t)$ and $u(t)$ are similar and each approximately 1. It also can be noticed that Fig. 4.15 shows that $u(t)$ and $r(t)$ compensate each other's dynamics, as they have opposite phase with one peaking when the other has a minimum, this would need further investigation.

4.8 Discussion

Overall, it is observed that three qubits give a richer quantum correlation landscape with two different types of entanglement. We discovered that depending on where one measures a qubit's occupation, one observes different dynamics, we named it delocalisation and localisation regimes.

The interplay between qubit dynamics and the depression mechanisms—though facilitation still needs further exploration—can be used to create prolonged entan-
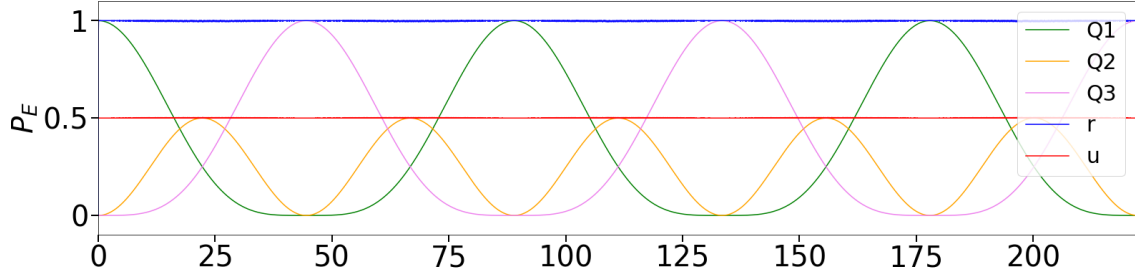
(a) Occupation probability. $\tau_d = 0.01$, $\tau_f = 0.01$, $U = 0.5$, $\Omega = 0.05$ and $\delta t = 0.01$ and measurement on Q_2.
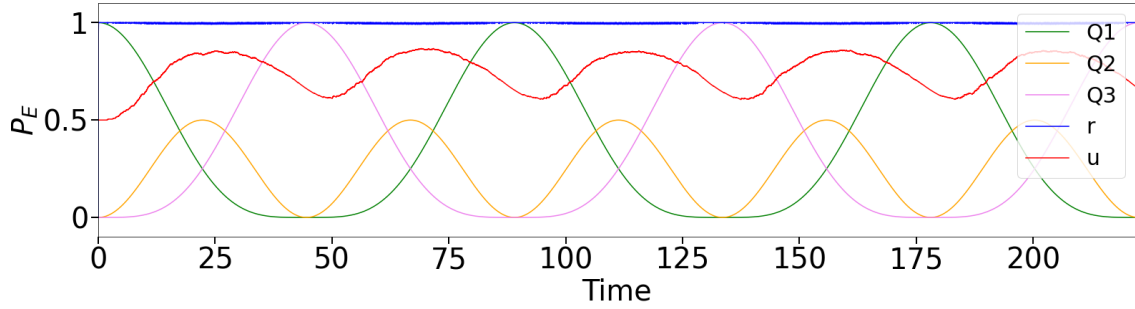
(b) Occupation probability. $\tau_d = 0.01$, $\tau_f = 10$, $U = 0.5$,$\Omega = 0.05$ and $\delta t = 0.01$ and measurement on Q_2.

Figure 4.13: Occupation probability versus time with facilitation with $\tau_f = \tau_d$ and $\tau_f \gg \tau_d$. τ.
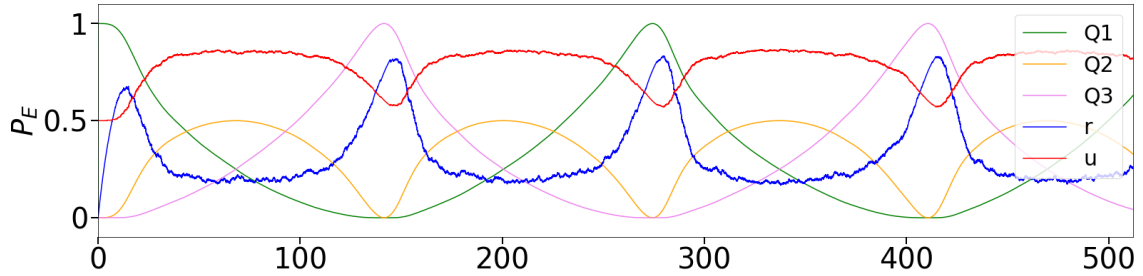
(a) Occupation probability. $\tau_d = 10$, $\tau_f = 10$, $U = 0.5$, $\Omega = 0.05$ and $\delta t = 0.01$ and measurement on Q_2.
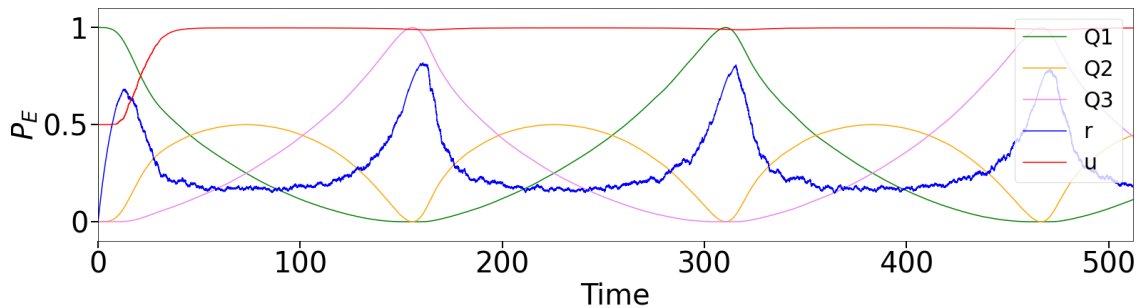
(b) Occupation probability. $\tau_d = 10$, $\tau_f = 1000$, $U = 0.5$ and $\delta t = 0.01$ and measurement on Q_2.

Figure 4.14: Occupation probability versus time with facilitation with $\tau_f = \tau_d$ and $\tau_f \gg \tau_d$. τ values much increased with respect to biological modelling.
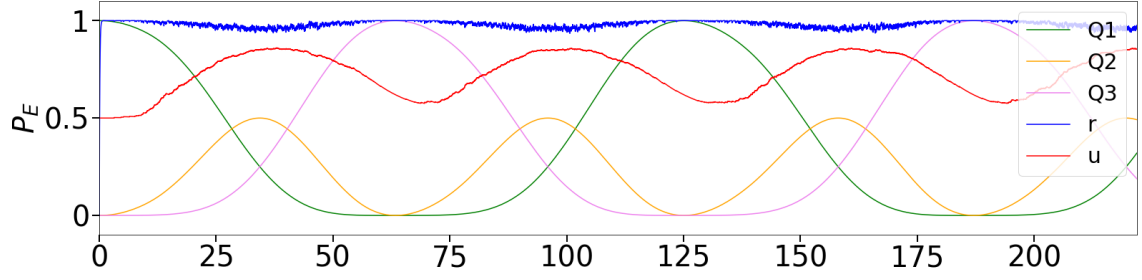
(a) Occupation probability with $r * u$ in the Hamiltonian. $\tau_d = 0.01$, $\tau_f = 10$, $U = 0.5$, $\Omega = 0.05$ and $\delta t = 0.01$ and measurement on Q_2.
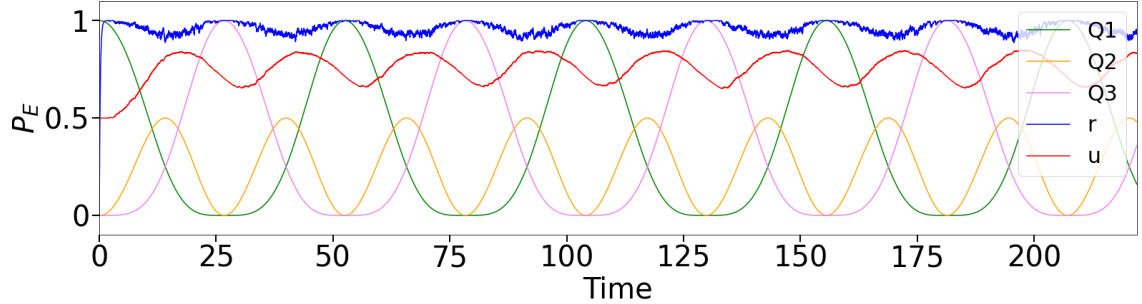
(b) Occupation probability with $r + u$ in the Hamiltonian. $\tau_d = 0.01$, $\tau_f = 10$, $U = 0.5$, $\Omega = 0.05$ and $\delta t = 0.01$ and measurement on Q_2.

Figure 4.15: Occupation probability vs time with Hamiltonian for $r * u$ (panel a) and $r + u$ (panel b)

glement in the system, allowing for long-lasting entanglement generation. By manipulating parameters such as depression, facilitation, and release probability, we can significantly alter the oscillation period of the chain across different time scales. Specifically, in certain conditions, just adjusting U can effectively increase the period, which may be beneficial.

A critical point to consider is the need to elaborate on how the Hamiltonian has been modified when facilitation is added in Eq. (4.10) and what facilitation contributes to. From the different runs when facilitation is added, we do not observe a significant impact of facilitation. When facilitation dominates ($\tau_f \gg \tau_d$), the original dynamics are recovered, suggesting that facilitation may not play a significant role under these specific conditions.

However, this observation raises a potential issue: maybe the quantum model, as it is, is not complete and requires modifications either in the Hamiltonian or the topology of the spin chain. We have already explored an alternative approach by adding $u(t)$ in the Hamiltonian, as shown in Fig. 4.15b and Fig. 4.15a. One could refer back to the classical model to identify any missing elements that might need to be integrated into the quantum model to observe a better interplay between facilitation and depression parameters.

Memory and Measurement: One possible solution would be to enable a feedback mechanism to observe different behaviour from the system, as shown in Fig. 4.16. This feedback mechanism could replicate the loop present in the phenomenological

model of synaptic working memory. Fig. 4.17 illustrates this process, where Ion Injection refers to ions, such as calcium ions (Ca2+), entering the presynaptic neuron during synaptic transmission. In the classical model, direct feedback loops may be required to retrieve memory in the biological context presented in this paper.
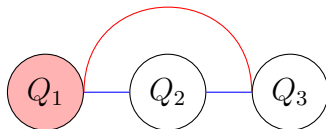
Figure 4.16: Three-qubits chain with excitation on Q_1 and feedback mechanism to enable facilitation in red and depression in blue.
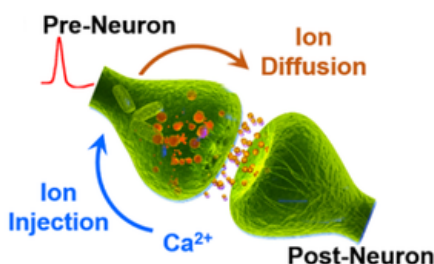
Figure 4.17: Representation of synaptic transmission highlighting the roles of ion diffusion and ion injection. In the synapse, the presynaptic neuron releases neurotransmitters through a process initiated by ion injection, specifically calcium (Ca2+) influx, which acts as a feedback loop to facilitate continuous neurotransmitter release. The released neurotransmitters diffuse across the synaptic cleft (ion diffusion) to the postsynaptic neuron, generating a new electrical signal. Illustration from [40].

Considering a simple linear chain scenario within a classical neural network, where three neurons are connected linearly without feedback loops, alternative network structures such as Synfire Chains [3] might be constructed from our spin chain, as shown in Fig. 4.18. These are feed-forward networks, with neurons organized across multiple layers. In a Synfire Chain, neural impulses are transmitted synchronously from one layer to the next. Though a linear structure might present challenges for memory capacity [36], it does not make memory retrieval impossible. Residual activity, even in the absence of recurrent connections, might still help retrieve memories, especially if retrieval is attempted shortly after encoding [60], [33].

Originally, we discussed that in the classical case, synapses between two neurons can either facilitate or depress. Facilitation, synonymous with strengthening, can help maintain information for a short period, with the information held in the synapses and retrieved at the postsynaptic neuron.

In a network with synaptic facilitation, such as depicted in Fig. 4.19, a set of excitatory neurons (representing one type of memory, for example, in blue) is linked as a subnetwork, while a set of inhibitory neurons forms a different subnetwork. The interplay between these networks (facilitation and depression) will aid memory retrieval, given an external cue, such as an attention probe.
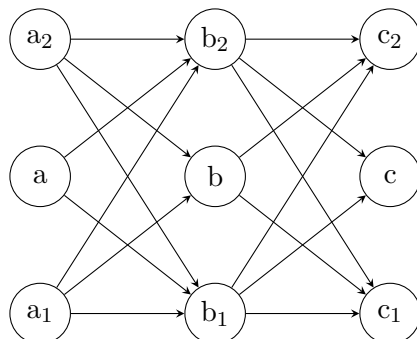
Figure 4.18: Illustration of formed synfire chain, where black arrows represent synapses, and circle neurons. Illustration from [74].
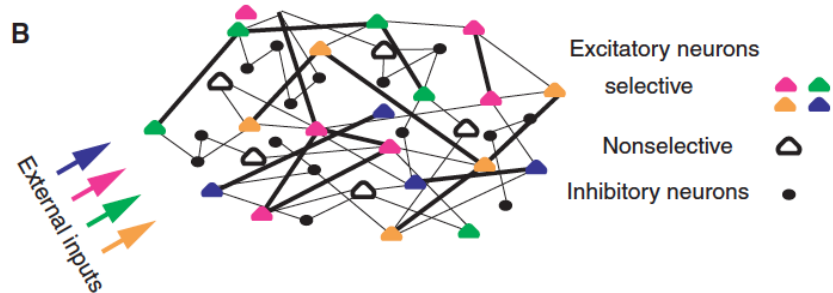
Figure 4.19: Network architecture. Colored triangles are excitatory neurons that code for different memories. Black open triangles are nonselective excitatory neurons. Black circles are inhibitory neurons with nonstructured connections to the entire network. Illustration from [48].
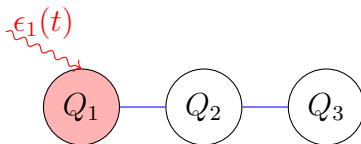
Figure 4.20: Three-qubits chain with excitation on Q_1 and time-depend on-site energy $\epsilon_1(t)$.

We now consider how this can be linked to quantum memory in our three-qubit system. The analogy involves maintaining information from different parts of the system, such as in Q_3, and optimising the conditions for information retention by either prolonging excitation or increasing its frequency. In this context, facilitation might not be necessary; instead, only the parameters τ and U may be required to achieve similar dynamics.

Another important aspect is the location of the measurement. In the working memory model, we do not have measurements, which could be considered as a mechanism for facilitation in our case. Referring to Fig. 4.6, in our scheme, the role of facilitation is done by measurement, making it the most effective method of facilitating.

Regarding entanglement, in this scenario, we destroy the entanglement between Q_1 and Q_3 because we localise all our excitation in one qubit, causing entanglement to decrease, only when $P_{E,Q} = 1$; otherwise the excitation is partly also in other qubits. But could entanglement be a measure of strength between two qubits, analogous to synaptic strength between two neurons? In our scenario having entanglement before localisation (time-wise) is connected to transferring information across the chain and hence between the two qubits.

However, in quantum mechanics, re-excitation is possible even without direct connections. Quantum evolution means that when part of the excitation is in Q_2, it can go both back to Q_1 and forward to Q_3, so in this respect, Q_1 does have the possibility of getting re-excited, even without a direct connection between 1 and 3.

Another possibility is to include facilitation with a time-dependent local potential, making one of the on-site energies time-dependent. This can be achieved using external fields, such as microwaves [11], depending on the physical implementation of the qubit [10]. This approach involves a different Hamiltonian, as shown in Fig. 4.20.

4.9   Chain with $N > 3$ qubits

In this section, initial results are presented for a spin chain of N̶ N qubits with perfect state transfer. For this analysis the code has been modified from the 3 qubit chains to be able to work with a generic number of qubits like in Fig. 4.21.
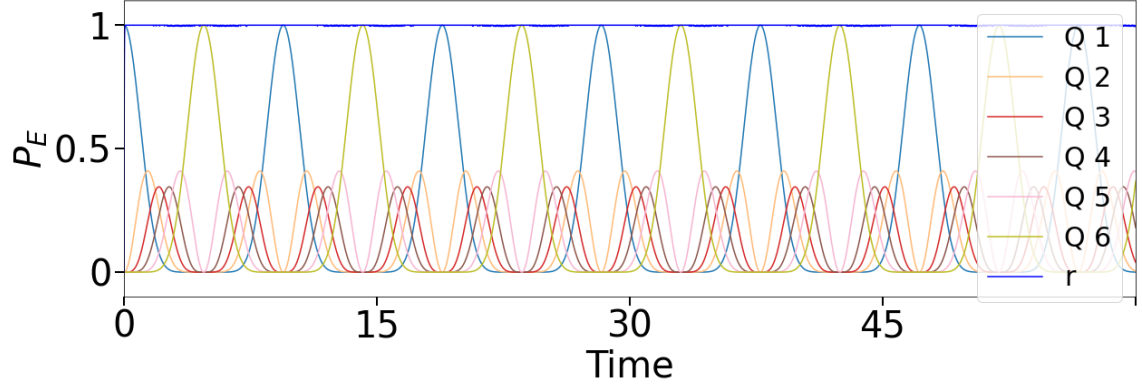
Figure 4.22: Occupation probability for 6 qubits with PST adjustment without depression. $\tau_d = 0.01$, $U = 0.5$ and $\delta t = 0.01$ and measurement on Q_2. Initial excitation on Q_1.
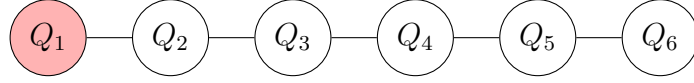
Figure 4.21: Six-qubits' chain with excitation on Q_1 (pink shade).

The Hamiltonian is of the form

$$H(t) = \frac{1}{2} \sum_{i,i+1} \Omega_{i,i+1} r_{i,i+1}(t) \left[\sigma_{x_i} \otimes \sigma_{x_{i+1}} + \sigma_{y_i} \otimes \sigma_{y_{i+1}} \right], \qquad (4.11)$$

where $\sigma_{x_i} \otimes \sigma_{x_{i+1}}$ is defined as

$$\sigma_{x_i} \otimes \sigma_{x_{i+1}} = \mathbb{I}_{1,i-1} \otimes \sigma_{x_i} \otimes \sigma_{x_{i+1}} \otimes \mathbb{I}_{i+2,N}, \qquad (4.12)$$

in this expression, $\mathbb{I}_{1,i-1}$ represents the identity matrix applied to the qubits from 1 to $i-1$, and $\mathbb{I}_{i+2,N}$ represents the identity matrix applied to the qubits from $i+2$ to N. This ensures that the operation only directly affects qubits i and $i+1$, with the rest of the qubits remaining unaffected by this particular interaction term. At any time, all couplings are rescaled by $r(t)$, such that $r_{i,i+1}(t) = r(t)$ for all i values.

$\Omega_{i,i+1}$ satisfy requirements for PST, and Eq. (2.9) discussed in Chapter 2 is used.

Preliminary results and discussion

Below are some preliminary results for depression only and the impact of depression values on occupation probability for a longer chain. The coupling values are: Ω_{0-1} : 0.745; Ω_{1-2} : 0.942; Ω_{2-3} : 1.0; Ω_{3-4} : 0.942; Ω_{4-5} : 0.745. These values are obtained with Eq. (2.9).

In the first instance, the results of the simulation for $N = 6$ qubits, shown in Fig. 4.22, resemble the probability occupation dynamics observed for three qubits. We observe periodicity and perfect state transfer between the first and last qubits, without any depression.
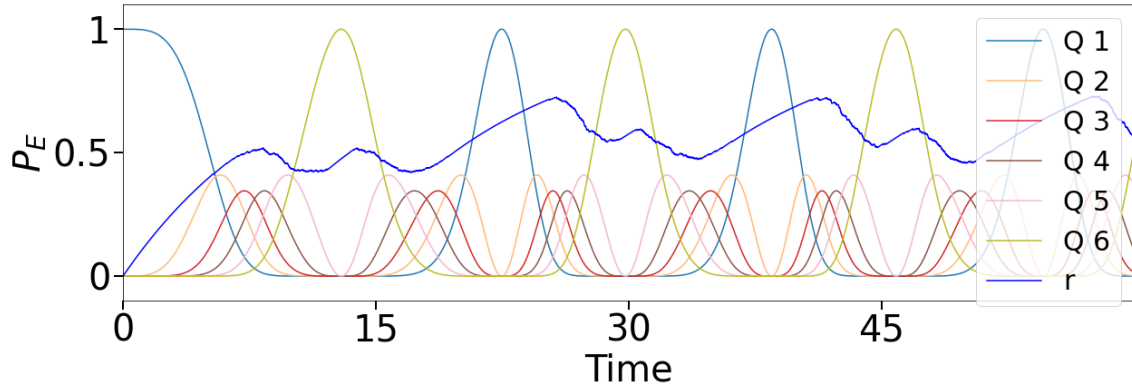
Figure 4.23: Occupation probability for 6 qubits with PST adjustment, with depression. $\tau_d = 10$, $U = 0.5$ and $\delta t = 0.01$ and measurement on Q_2. Initial excitation on Q_1.
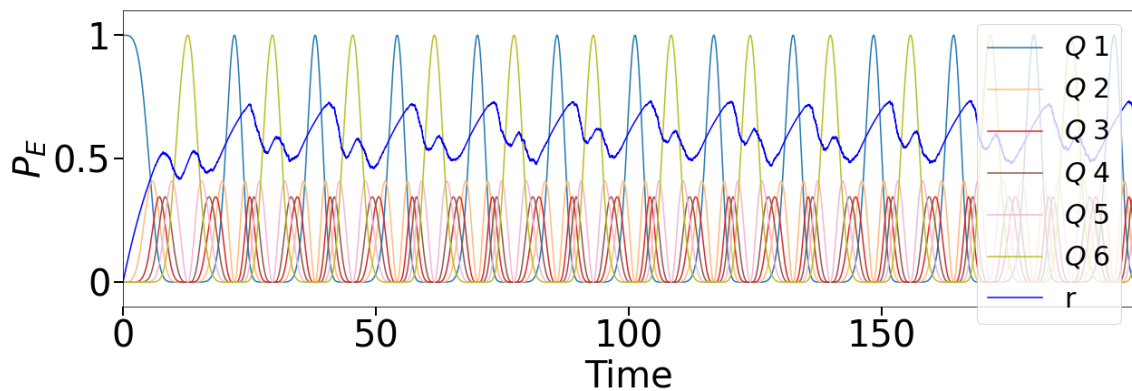
Figure 4.24: Occupation probability for 6 qubits with PST adjustment for a longer time. Parameters are set to $\tau_d = 10$ and $\delta t = 0.01$, with measurement on Q_2 and initial excitation on Q_1.
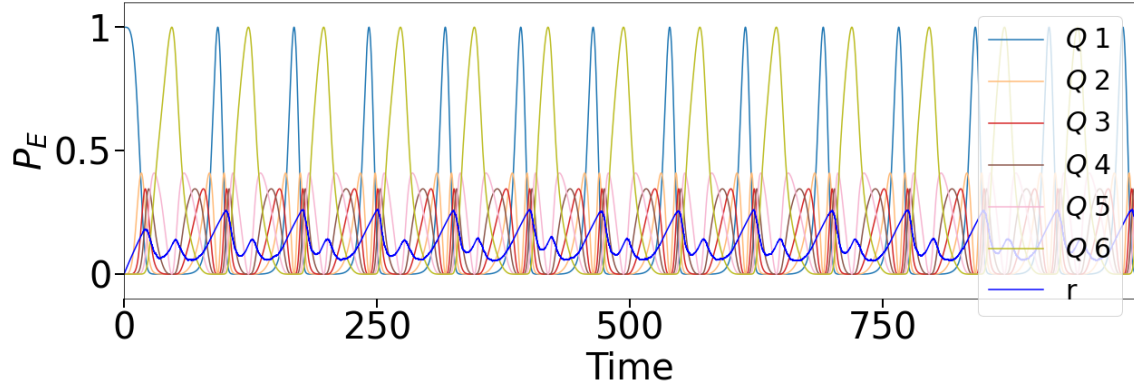
Figure 4.25: Occupation probability for 6 qubits with PST adjustment for a longer time. Parameters are set to $\tau_d = 100$, $U = 0.5$, and $\delta t = 0.01$, with measurement on Q_2 and initial excitation on Q_1.
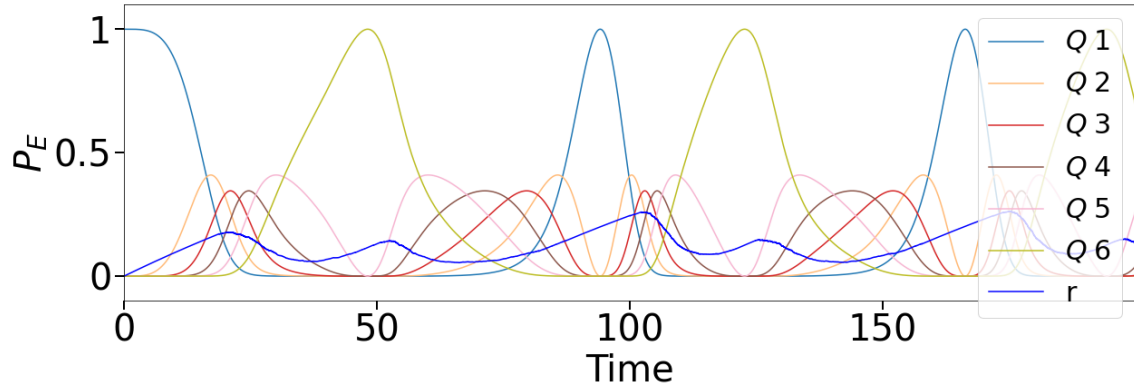
Figure 4.26: Zoomed view: Occupation probability for 6 qubits with PST adjustment for a longer time. Parameters are set to $\tau_d = 100$, $U = 0.5$, and $\delta t = 0.01$, with measurement on Q_2 and initial excitation on Q_1.

However, when we set $\tau_d = 10$ to introduce depression, a transient period can be observed. For example, the transient period lasts until approximately t $\approx$ 15 units of time, as shown in Fig. 4.23.

The two graphs Fig. 4.24 and Fig. 4.25 demonstrate the impact of chain length on the transient period and regular periodicity in a 6-qubit spin chain, while the system still achieves perfect state transfer, ensuring the high-fidelity transfer of quantum states. Each qubit interacts with its neighbors, and the information must propagate sequentially through the chain. This sequential propagation introduces a delay before the entire system reaches a synchronized periodic state. This is made obvious in Fig. 4.25. The longer transient period observed is due to the increased time required for information to propagate through the chain. In contrast, shorter chains would exhibit quicker stabilisation and shorter transient periods due to more efficient information transfer.

By analysing the graphs for $\tau_d = 100$ in Fig. 4.25 and Fig. 4.26, we notice that the transient period lasts until approximately t $\approx$ 100 units of time. Despite the longer transient period due to the increased τ_d, the system eventually achieves regular periodicity, ensuring high-fidelity transfer of quantum states from one end of the

chain to the other.

Chapter 5

Conclusions

Throughout this thesis, we have taken the first steps toward investigating a complex system, building on previous research. We examined how the addition of increasingly dynamic elements in the system Hamiltonian, such as adding more qubits, introducing facilitation, or using different measurements across the chain, can impact the transfer of information across a linear spin chain.

5.1   Discussion

From our results we can conclude that the excitation requires more time to propagate through the chain from the first qubit to the last when there is a decrease in activity. For larger τ_d values, we have less time with respect to the period length to do precise measurements due to the time in which the excitation stays localised. The decrease in activity doesn't block information transmission; rather, it slows it down, reducing the probability of accurately measuring the excitation. Therefore, greater care is needed in these measurements.

One significant finding is that the location of qubit measurement directly influences the system's dynamics, particularly affecting the phenomena of localisation and delocalisation.

Interestingly, increasing depression in the system does not block information transfer, as in the classical case; instead, it slows the transfer down, and by inducing a delocalisation regime, reduces the likelihood of measuring the transferred excitation. This calls for more precision in measurement techniques.

The effect of facilitation that was observed in our simulation results is very similar to the one observed with depression. In the classical working memory model employed, there is a feedback loop mechanism that could potentially contribute to facilitation effects. Therefore, it might be beneficial to incorporate this feedback loop explicitly into the quantum model to investigate whether it leads to a more substantial facilitation effect.

5.2 Future direction

The topic of this thesis is not a widely developed area, so there are many avenues to explore. We should not lose track of the motivation for this research, which is using our current understanding of neuroscience and examining how well it can be transferred to the field of quantum technologies.

We have started to look in more depth at a model of short-term synaptic plasticity using two coupled differential equations and how it can be of use in the transfer of quantum states. We also noticed that with just a few input variables and additional network complexity the model can become difficult to understand and may require different tools or theoretical approaches to explore the model dynamic behavior and its computational implications [69].

The encouraging results could lead us to further explore the model of synaptic plasticity, expanding it with various network topologies to make it more like a network of neurons. It is important not to forget the early models of neural networks, such as the Hopfield network, which is directly inspired by spin glasses [39]. We also have the capability to add the effects of temperature on the system and use the methods of quantum thermodynamics to observe its impact.

We could also investigate how memories are stored and retrieved in a classical model and see how this can be applied to quantum information. Our brain is a noisy environment, and there is evidence that slender axons where information propagates, are more susceptible to noise [55], which directly impacts how our cognitive system operates [54]. To describe this within a quantum system, one could consider disorder or imperfections in the values of the qubit couplings ($\Omega_{i,i+1}$) and their relative sizes [61]. Finally, we could potentially collaborate with experimentalists in the future to implement these ideas and validate that the theory can be applied to real-world systems.

Additionally, one could simulate techniques such as chirped pulse amplification, which generates high-intensity, ultrashort pulses capable of producing different frequencies within a single pulse [65]. This simulation could represent various spiking intervals. For example, Fig. 5.4 in appendix A, illustrates different spiking intervals for the classical model and we could examine how these intervals impact the quantum version.

By exploring the parallels between neuroscience and quantum systems, we hope to find improvements and discoveries of new functionalities for quantum technology, particularly in networks of qubits to advance the capabilities in this field.

Appendix

5.3 Original phenomenological model of synaptic depression only

The model presented in this appendix is characterised by three variables and equations instead of one for the depression model. However the single differential equation for depression used in this work can be recovered. The facilitation part can also be added, additional details can be found in [37].

The central concept of the model is that each synaptic connection between neurons, can be defined by its total 'resources', which are divided into three states: active, inactive, and recovered, see Fig. 5.1.

We will work with our notation, the original paper notation [37] is slightly different. Let r (x in the original notation) be the fraction of neurotransmitters which is recovered after a previous arrival of an action potential near the cell membrane, y is the fraction of neurotransmitters which is released into the synaptic cleft after the arrival of an action potential and z is fraction of inactive neurotransmitters, this follows the dynamics.

Recovered

$$\frac{dr}{dt} = \frac{z}{\tau_{\text{rec}}} - Ur\delta\left(t - t_{\text{sp}}\right). \tag{5.1}$$

Active

$$\frac{dy}{dt} = \frac{-y}{\tau_{\text{in}}} + Ur\delta\left(t - t_{\text{sp}}\right). \tag{5.2}$$

Inactive

$$\frac{dz}{dt} = \frac{y}{\tau_{\text{rec}}} - \frac{z}{\tau_{\text{in}}}. \tag{5.3}$$

Diagram explanation

- Recovered (r) to Active (y): When a spike occurs, a fraction $Ur\delta(t - t_{sp})$ of the recovered resources becomes active.

- Active (y) to Inactive (z): The active resources decay to the inactive state with a time constant τ_{in}, represented by $\frac{y}{\tau_{in}}$.
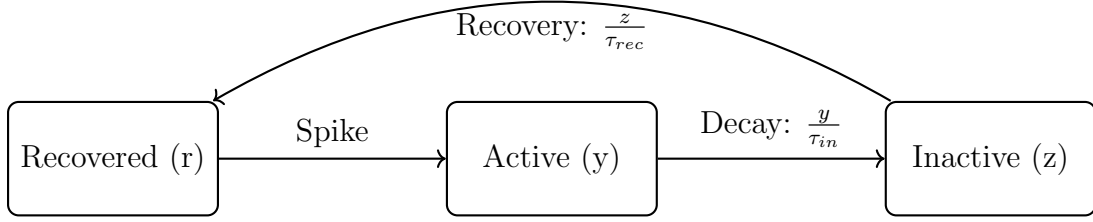
Figure 5.1: Flow of synaptic resources between states.

- Inactive (z) to Recovered (r) The inactive resources recover to the recovered state with a time constant τ_{rec}, represented by $\frac{z}{\tau_{rec}}$.

- The model assumes total conservation of neurotransmitter resources (normalisation condition)

$$r + y + z = 1. \tag{5.4}$$

- For constant release probability U, the model describes the basic mechanism of synaptic depression. If $U = u(t)$ is time dependent the model describes as well facilitation.

Equation (5.1) can be simplified substantially if one takes into account that realistically $\tau_{in} \ll \tau_{rec}$ (about $1s$ τ_{rec} and few milliseconds for τ_{in}) and the rate of the incoming spike train is usually much lower than $1/\tau_{in}$.

Taken together with the normalisation condition $z = 1 - r - y$ this allows to reduce Eq. (5.1) with a single equation for r.

$$\frac{dr}{dt} = \frac{1-r}{\tau_{\text{rec}}} - \frac{y}{\tau_{\text{rec}}} - Ur\delta\left(t - t_{\text{sp}}\right). \tag{5.5}$$

To recover the equation for depression Eq. (2.1) we need to justify why the term $\frac{-y}{\tau_{\text{rec}}}$ can be neglected.

We know that $\frac{1}{\tau_{rec}} \ll \frac{1}{\tau_{in}}$ and $\frac{-y}{\tau_{\text{in}}}$ is large and negative, so that it causes $y(t)$ to decay exponentially very fast in Eq. (5.2) . This can be seen in Fig. 5.2 for $y(t)$. There we plot the solution of a first-order linear ordinary differential equation

$$y(t) = Ae^{-\frac{t}{\tau_{\text{in}}}}, \tag{5.6}$$

where A is the initial value of y at $t = 0$. This solution describes exponential decay of y over time with a decay constant of τ_{in}.

The graph Fig. 5.3 illustrates the dynamics of synaptic resource states over time, with an emphasis on how these states change in response to periodic spikes. The states include the recovered state (r), the active state (y), and the inactive state (z). Additionally, the graph shows the average value of the active state (y_{avg}) over one period.

The initial spike at $t = 0$ results in an immediate increase in the active state (y) to 0.2 (U). Subsequent spikes show similar behavior, with the active state (y) increasing
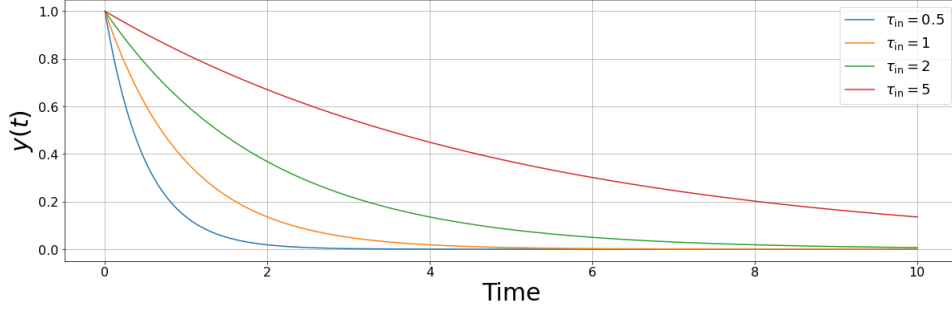
Figure 5.2: $y(t)$ from equation 5.6
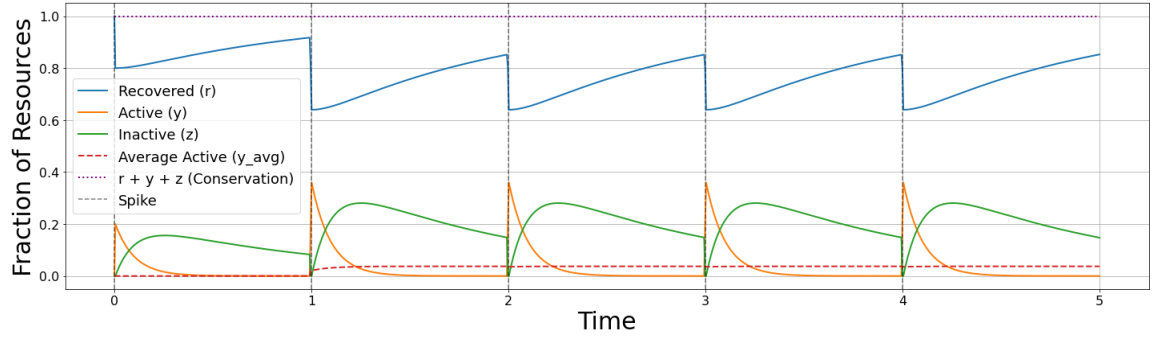
Figure 5.3: Dynamics of synaptic decay, with fraction of resources versus time and $U = 0.2$ with conservation probability in Eq. 5.4.

by $U \times r$, where r is the fraction of recovered resources available at the time of the spike. If the active state (y) does not fully decay to zero between spikes, the next spike will add to the remaining active resources, potentially causing higher peaks. It can then be noticed that (y_{avg}) over long period is negligible due to the fast decay in between each spike, this is due to the condition that the rate of the incoming spike train is usually much lower than $1/\tau_{in}$.

Therefore the dynamics of equation Eq. (5.1) depends on the rate of decay of $y(t)$. One can then let $\frac{-y}{\tau_{\mathrm{rec}}}$ goes to 0 ($y(t)$ is small for t big enough).

We recover therefore the equation for depression with $\tau_{rec} = \tau_d$

$$\frac{dr}{dt} = \frac{1-r}{\tau_{rec}} - Ur\delta\left(t - t_{sp}\right). \tag{5.7}$$

In the graph Fig.5.4, we plot the effect of different spiking rates for the fraction of active resources $y(t)$. This illustrates the condition where the rate of the incoming spike train is usually much lower than $1/\tau_{\mathrm{in}}$, allowing $y(t)$ to decay to zero between spikes. Conversely, if the spiking rate is too high, we observe the opposite effect.
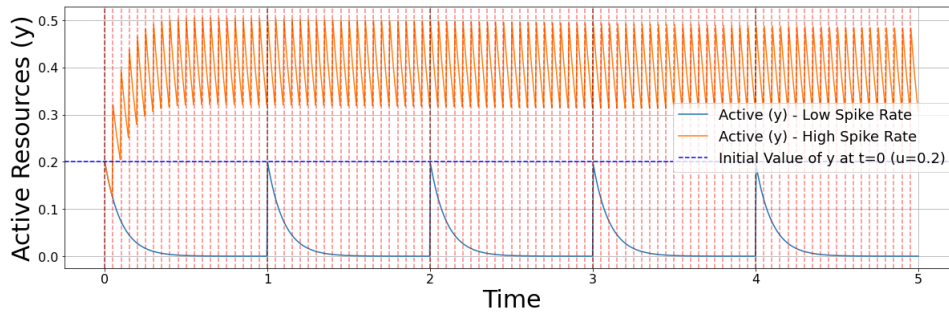
Figure 5.4: Fraction of active resources $y(t)$ for $U = 0.2$ and different spike rate over time, with $1\,\mathrm{Hz}$ (spike interval of $1.0\,\mathrm{s}$); high spike rate: $20\,\mathrm{Hz}$ (spike interval of $0.05\,\mathrm{s}$). In light blue, a slow spiking train; in red, a faster spiking rate.

5.4 Pseudoalgorithms

The first pseudoalgorithm outlines the overall structure for a 3-qubit spin chain, with the various functions used to simulate the excitation probability evolution and the entanglement dynamics evolution. For simplicity, the other detailed calculations and plots are not included.

The second pseudoalgorithm describes the calculation for single-site entanglement and entanglement between qubits. Currently, the code only works for three qubits to compute the entanglment. This needs to be reviewed for an N-qubit implementation.

Algorithm 1 Example of code for a 3 qubit spin chain

1: Example of parameters: $r_0 \leftarrow 0$, $\tau \leftarrow 0.01$, $dt \leftarrow 0.01$, $t_{max} \leftarrow 222$, $U \leftarrow 0.5$
2: Define Hamiltonian diagonal elements: diagonal_H $\leftarrow [-3, -1, -1, 1, -1, 1, 1, 3]$
3: Initialize results dictionaries: results
4: all_negativity_1
5: all_negativity_2
6: all_negativity_3
7: all_negativity_4
8: **procedure** RHO_DERIVATIVE(H, ρ)
9:     **return** $-1i \cdot H \cdot \rho + 1i \cdot \rho \cdot H$
10: **end procedure**
11: **procedure** RUNGE_KUTTA_4$(r_{prev}, \rho_{prev}, H_{prev}, H\_func, dt, \tau, U, S)$
12:     Calculate k_1 for r and ρ
13:     Calculate k_2 using mid-point values
14:     Calculate k_3 using mid-point values
15:     Calculate k_4 using next values
16:     Combine k_1, k_2, k_3, k_4 to estimate r_{new}, ρ_{new}
17:     **return** $r_{new}, \rho_{new}, H_{next}$
18: **end procedure**
19: **procedure** H_FUNC(r)
20:     **return** Hamiltonian matrix based on r and diagonal_H
21: **end procedure**
22: **procedure** INTEGRATE_EQUATION$(r_0, \tau, U, dt, t_{max})$
23:     Initialize $tpoints, r, H, \rho$
24:     Set initial conditions for ρ
25:     Initialize $\rho_{00}, \rho_{11}, \rho_{22}, \rho_{33}, \rho_{44}, \rho_{55}, \rho_{66}, \rho_{77}$
26:     Initialize negativity lists
27:     **for** $i \in 1$ to $len(tpoints)$ **do**
28:         Generate random x and set S
29:         Update $r[i], \rho[i], H[i]$ using Runge-Kutta method
30:         Normalize $\rho[i]$
31:         Extract diagonal elements of $\rho[i]$
32:         Compute negativity for different partitions of the system
33:     **end for**
34:     **return** $tpoints, negativity\_lists, r, \rho_{elements}$
35: **end procedure**
36: **for** $U \in U\_values$ **do**
37:     Run simulation and store results
38:     Print completion message for U
39: **end for**

Algorithm 2 Calculation of negativities for single site and between end qubits entanglement

---

1: **procedure** COMPUTE_NEGATIVITY_1(ρ)
2:      $\rho_1 \leftarrow$ partial transpose of ρ with respect to system $1|23$
3:      eigenvalues_1 $\leftarrow$ eigvals(ρ_1)
4:      negativity_1 $\leftarrow 0.5 \times (\sum \text{abs(eigenvalues\_1)} - 1)$
5:      append negativity_1 to list
6: **end procedure**
7: **procedure** COMPUTE_NEGATIVITY_3(ρ)
8:      $\rho_3 \leftarrow$ partial transpose of ρ with respect to system $12|3$
9:      eigenvalues_3 $\leftarrow$ eigvals(ρ_3)
10:      negativity_3 $\leftarrow 0.5 \times (\sum \text{abs(eigenvalues\_3)} - 1)$
11:      append negativity_3 to list
12: **end procedure**
13: **procedure** COMPUTE_NEGATIVITY_2(ρ)
14:      $\rho_2 \leftarrow$ partial transpose of ρ with respect to system $13|2$
15:      eigenvalues_2 $\leftarrow$ eigvals(ρ_2)
16:      negativity_2 $\leftarrow 0.5 \times (\sum \text{abs(eigenvalues\_2)} - 1)$
17:      append negativity_2 to list
18: **end procedure**
19: **procedure** COMPUTE_NEGATIVITY_4(ρ)
20:      $\rho_4 \leftarrow$ reduced density matrix of ρ tracing out q2
21:      $\rho_{PT} \leftarrow$ partial transpose of ρ_4 with respect to subsystem q1
22:      eigenvalues_4 $\leftarrow$ eigvals(ρ_{PT})
23:      negativity_4 $\leftarrow 0.5 \times (\sum \text{abs(eigenvalues\_4)} - 1)$
24:      append negativity_4 to list
25: **end procedure**

Acronyms

- τ_d: Time constant for depression

- τ_f: Time constant for facilitation

- U: Baseline release probability

- $u(t)$: Instantaneous release probability

- $r(t)$: Amount of available resources

- Ω: Qubits interaction strength

- P_E: Qubit excitation probability

- $\epsilon_1(t)$: On-site energy

- LR: Localisation regime

- DR: Delocalisation regime

- Q_2: Qubit 2

- $N_{ss}^{Q_i}(t)$: Negativity, single site entanglement

- $N_{qq}^{Q_i}(t)$: Negativity, qubit to qubit entanglement

- T_{tr}: Transfer time between 2 qubits (averaged over 3 consecutive periods)

- δt: Time step used for numerical integration

Bibliography

[1]   Amira Abbas et al. "The power of quantum neural networks". In: *Nature Computational Science* 1.6 (2021), pp. 403–409.

[2]   Laurence F. Abbott and Peter Dayan. *Theoretical Neuroscience: Computational and Mathematical Modeling of Neural Systems.* 1st. Cambridge, MA: The MIT Press, 2001, p. 480. ISBN: 978-0262041997.

[3]   Moshe Abeles. *Corticonics: Neural Circuits of the Cerebral Cortex.* Cambridge, UK: Cambridge University Press, 1991.

[4]   C. Albanese et al. "Mirror Inversion of Quantum States in Linear Registers". In: *Physical Review Letters* 93.23 (2004), p. 230502. DOI: 10.1103/PhysRevLett.93.230502.

[5]   Abdulsalam H. Alsulami et al. "Scalable Quantum Spin Networks from Unitary Construction". In: *Advanced Quantum Technologies* 7.2 (2024), p. 2300238.

[6]   Abdulsalam H. Alsulami et al. "Unitary Design of Quantum Spin Networks for Robust Routing, Entanglement Generation, and Phase Sensing". In: *Advanced Quantum Technologies* 5.8 (2022), p. 2200013.

[7]   N. S. Babcock et al. "Ultraviolet Superradiance from Mega-Networks of Tryptophan in Biological Architectures". In: *The Journal of Physical Chemistry B* 128.17 (May 2024), pp. 4035–4046.

[8]   K.K. Berggren. "Quantum computing with superconductors". In: *Proceedings of the IEEE* 92.10 (2004), pp. 1630–1638.

[9]   Abdulfateh Bezaz. "Perfect state transfer in spin-chains with on-site energy parametrization". 2023. URL: https://etheses.whiterose.ac.uk/33045/.

[10] Alexandre Blais, Alexander Maassen van den Brink, and Alexandre M. Zagoskin. "Tunable Coupling of Superconducting Qubits". In: *Physical Review Letters* 90.12 (Mar. 2003). ISSN: 1079-7114.

[11] Alexandre Blais et al. "Circuit quantum electrodynamics". In: *Rev. Mod. Phys.* 93 (2 2021), p. 025005.

[12] A. Blanco-Redondo et al. "Topological Optical Waveguiding in Silicon and the Transition between Topological and Trivial Defect States". In: *Physical Review Letters* 116 (2016), p. 163901.

[13] Sougato Bose. "Quantum communication through spin chain dynamics: an introductory overview". In: *Contemporary Physics* 48.1 (2007), pp. 13–30.

[14] B. H. Bransden. *Quantum Mechanics.* 2nd ed. Pearson, 2000.

[15] Benjamin J. Brown and Sam Roberts. "Universal fault-tolerant measurement-based quantum computation". In: *Phys. Rev. Res.* 2 (3 2020), p. 033305.

[16] Kenneth R Brown, Jungsang Kim, and Christopher Monroe. "Co-designing a scalable quantum computer with trapped atomic ions". In: *npj Quantum Information* 2.1 (2016), p. 16034.

[17] R. Brunner et al. "Two-Qubit Gate of Combined Single-Spin Rotation and Interdot Spin Exchange in a Double Quantum Dot". In: *Physical Review Letters* 107.14 (2011), p. 146801.

[18] Daniel Burgarth and Sougato Bose. "Conclusive and arbitrarily perfect quantum-state transfer using parallel spin-chain channels". In: *Phys. Rev. A* 71 (5 2005), p. 052315.

[19] Guido Burkard, Daniel Loss, and David P. DiVincenzo. "Coupled quantum dots as quantum gates". In: *Physical Review B* 59.3 (1999), pp. 2070–2078.

[20] Jiu-Peng Chen et al. "Sending-or-Not-Sending with Independent Lasers: Secure Twin-Field Quantum Key Distribution over 509 km". In: *Phys. Rev. Lett.* 124 (7 2020), p. 070501.

[21] Matthias Christandl et al. "Perfect State Transfer in Quantum Spin Networks". In: *Phys. Rev. Lett.* 92 (18 2004), p. 187902.

[22] Nelson Cowan. "Chapter 20 What are the differences between long-term, short-term, and working memory?" In: Progress in Brain Research 169 (2008). Ed. by Wayne S. Sossin et al., pp. 323–338.

[23] Irene D'Amico. "Quantum dot-based quantum buses for quantum computer hardware architecture". In: *Microelectronics Journal* 37.12 (2006), pp. 1440–1441.

[24] Irene D'Amico, Brendon W Lovett, and Timothy P Spiller. "Freezing distributed entanglement in spin chains". English. In: *Physical Review A* 76.3 (2007). ISSN: 1050-2947.

[25] Jonathan Daume et al. "Control of working memory by phase–amplitude coupling of human hippocampal neurons". In: *Nature* (2024).

[26] Albert Einstein, Boris Podolsky, and Nathan Rosen. "Can Quantum-Mechanical Description of Physical Reality Be Considered Complete?" In: *Physical Review* 47.10 (1935), pp. 777–780.

[27] A. Ekert et al. "Quantum computation in brain microtubules? The Penrose–Hameroff 'Orch OR' model of consciousness". In: *Philosophical Transactions of the Royal Society of London. Series A: Mathematical, Physical and Engineering Sciences* 356.1743 (1998), pp. 1869–1896.

[28] Roland Ennos. *The Science of Spin: The Force Behind Everything – From Falling Cats to Jet Engines.* Oneworld Publications, 2023.

[29] Marta P Estarellas, Timothy P Spiller, and Irene D'Amico. "Comparison of entangling protocols in ABC-type spin chains". In: *Journal of Physics: Conference Series* 1638.1 (2020), p. 012013.

[30] Marta P. Estarellas, Irene D'Amico, and Timothy P. Spiller. "Topologically protected localised states in spin chains". In: *Scientific Reports* 7.1 (2017), p. 42904.

[31] Pascual Estarellas. "Spin chain systems for quantum computing and quantum information applications". 2018. URL: https://etheses.whiterose.ac.uk/20556/.

[32] Johannes Franke et al. "Quantum-enhanced sensing on optical transitions through finite-range interactions". In: *Nature* 621.7980 (2023), pp. 740–745.

[33] Paul W. Frankland, Sheena A. Josselyn, and Stefan Köhler. "The neurobiological foundation of memory retrieval". In: *Nature Neuroscience* 22.10 (2019), pp. 1576–1585.

[34] J M Fuster. "Unit activity in prefrontal cortex during delayed-response performance: neuronal correlates of transient memory." In: *Journal of Neurophysiology* 36.1 (1973), pp. 61–78.

[35] Tasio Gonzalez-Raya et al. "Quantized Single-Ion-Channel Hodgkin-Huxley Model for Quantum Neurons". In: *Phys. Rev. Appl.* 12 (1 2019), p. 014037.

[36] Sarah Greberman, Yevhen Tupikov, and Dezhe Jin. "Exploring the Memory Capacity of Embedded Synfire Chains". In: *APS March Meeting 2020*. Abstract C71.00074. American Physical Society. 2020. URL: https://meetings.aps.org/Meeting/MAR20/Session/C71.74.

[37] Gutkin Hansel. "Lecture Notes of the Les Houches Summer School 2003". In: Methods and Models in Neurophysics: 80 (2004). Ed. by Wayne S. Sossin et al., pp. 323–338.

[38] Werner Heisenberg. "Zur Theorie des Ferromagnetismus". In: *Zeitschrift für Physik* 49.9-10 (1928), pp. 619–636.

[39] John J. Hopfield. "Neural networks and physical systems with emergent collective computational abilities". In: *Proceedings of the National Academy of Sciences* 79.8 (1982), pp. 2554–2558.

[40] Xinglong Ji et al. "Artificial Working Memory Constructed by Planar 2D Channel Memristors Enabling Brain-Inspired Hierarchical Memory Systems". In: *Advanced Intelligent Systems* 4.3 (2022), p. 2100119.

[41] Alastair Kay. "Perfect, Efficient, State Transfer and Its Application as a Constructive Tool". In: *International Journal of Quantum Information* 8.04 (2010), pp. 641–676. DOI: 10.1142/S0219749910006514.

[42] Lasse Bjørn Kristensen et al. "An artificial spiking quantum neuron". In: *npj Quantum Information* 7.1 (2021), p. 59.

[43] S. Kulkarni. "The Science of 3 Body Problem: What's Fact and What's Fiction?" In: *Nature* (2024). Advance online publication.

[44] S. Lorenzo et al. "Quantum-state transfer via resonant tunneling through local-field-induced barriers". In: *Physical Review A* 87.4 (2013), p. 042313.

[45] S. Lorenzo et al. "Quantum-state transfer via resonant tunneling through local-field-induced barriers". In: *Phys. Rev. A* 87 (4 2013), p. 042313.

[46] Daniel Loss and David P. DiVincenzo. "Quantum computation with quantum dots". In: *Phys. Rev. A* 57 (1 1998), pp. 120–126.

[47] Robert C. Malenka and Roger A. Nicoll. "Long-term potentiation—a decade of progress?" In: *Science* 285.5435 (1999), pp. 1870–1874. DOI: 10.1126/science.285.5435.1870.

[48] Gianluigi Mongillo, Omri Barak, and Misha Tsodyks. "Synaptic Theory of Working Memory". In: *Science* 319.5869 (2008), pp. 1543–1546.

[49] R.G.M Morris. "D.O. Hebb: The Organization of Behavior, Wiley: New York; 1949". In: *Brain Research Bulletin* 50.5 (1999), p. 437.

[50] Georgios M. Nikolopoulos, David Petrosyan, and Peter Lambropoulos. "Electron wavepacket propagation in a chain of coupled quantum dots". In: *Journal of Physics: Condensed Matter* 16.28 (2004), p. 4991.

[51] T. E. Northup and R. Blatt. "Quantum information transfer using photons". In: *Nature Photonics* 8.5 (2014), pp. 356–363.

[52] T. Ohshima et al. "Robust state transfer and rotation through a spin chain via dark passage". In: *arXiv preprint arXiv:0702019* (2007). Available online: https://arxiv.org/abs/0702019.

[53] Tobias J. Osborne and Noah Linden. "Propagation of quantum information through a spin system". In: *Phys. Rev. A* 69.5 (2004), p. 052315.

[54] Tim Palmer. *The Primacy of Doubt: From Quantum Physics to Climate Change, How the Science of Uncertainty Can Help Us Understand Our Chaotic World*. New York: Basic Books, 2022. ISBN: 9781541619715.

[55] Tim N. Palmer and Michael O'Shea. "Solving difficult problems creatively: a role for energy optimised deterministic/stochastic hybrid computing". In: *Frontiers in Computational Neuroscience* 9 (2015).

[56] Asher Peres. "Separability Criterion for Density Matrices". In: *Phys. Rev. Lett.* 77 (8 1996), pp. 1413–1415.

[57] *Quantum State Transfer and Network Engineering*. Springer Berlin Heidelberg, 2014. ISBN: 9783642399374.

[58] Giovanni Ramírez, Javier Rodríguez-Laguna, and Germán Sierra. "Entanglement over the rainbow". In: *Journal of Statistical Mechanics: Theory and Experiment* 2015.6 (2015), P06002.

[59] Jan Riegelmeyer et al. "Generation and robustness of quantum entanglement in spin graphs". In: *Quantum Information Processing* 20.1 (2020), p. 2.

[60] Henry L. Roediger and Magdalena Abel. "The double-edged sword of memory retrieval". In: *Nature Reviews Psychology* 1.12 (2022), pp. 708–720.

[61] Rebecca Ronke et al. "Anderson localisation in spin chains for perfect state transfer". In: *The European Physical Journal D* 70.9 (2016), p. 189.

[62] Indubala I. Satija. *The Wonder of Quantum Spin: The Discovery, Evolution, and Mathematics of Spin*. Oxford University Press, 2024. ISBN: 9780198884853.

[63] Benjamin Schumacher. "Quantum coding". In: *Physical Review A* 51.4 (1995), pp. 2738–2747.

[64] Mark G. Stokes. "'Activity-silent' working memory in prefrontal cortex: a dynamic coding framework". In: *Trends in Cognitive Sciences* 19.7 (2015), pp. 394–405.

[65] Donna Strickland and Gerard Mourou. "Compression of amplified chirped optical pulses". In: *Optics Communications* 56.3 (1985), pp. 219–221.

[66] Yu-Juan Sun and Wei-Min Zhang. "Modeling Neuronal Systems as an Open Quantum System". In: *Symmetry* 13.9 (2021).

[67] Francesco Tacchino et al. "An artificial neuron implemented on an actual quantum processor". In: *npj Quantum Information* 5.1 (2019), p. 26.

[68] J J Torres and D Manzano. "A model of interacting quantum neurons with a dynamic synapse". In: *New Journal of Physics* 24.7 (2022), p. 073007.

[69] J.J. Torres and H.J. Kappen. "Emerging phenomena in neural networks with dynamic synapses and their computational implications". In: *Frontiers in Computational Neuroscience* 7 (2013), p. 30.

[70] Raju Valivarthi et al. "Teleportation Systems Toward a Quantum Internet". In: *PRX Quantum* 1 (2 2020), p. 020317.

[71] G. Vidal and R. F. Werner. "Computable measure of entanglement". In: *Phys. Rev. A* 65 (3 2002), p. 032314.

[72] Yun Wang et al. "Heterogeneity in the pyramidal network of the medial prefrontal cortex". In: *Nature Neuroscience* 9.4 (2006), pp. 534–542.

[73] B. P. Williams, R. J. Sadlier, and T. S. Humble. "Superdense Coding over Optical Fiber Links with Complete Bell-State Measurements". In: *Physical Review Letters* 118.5 (2017), p. 050501.

[74] Pengsheng Zheng and Jochen Triesch. "Robust development of synfire chains from multiple plasticity mechanisms". In: *Frontiers in Computational Neuroscience* 8 (2014).

[75] Robert S. Zucker and Wade G. Regehr. "Short-Term Synaptic Plasticity". In: *Annual Review of Physiology* 64.Volume 64, 2002 (2002), pp. 355–405.